# Cornell University

Soft-Robotic Rover with Electrodynamic Power Scavenging

NIAC Phase 1 Final Report

Cornell University

3/9/2016

1   Contents

2   Executive Summary

The purpose of studying the capabilities of Electrodynamic Tethers (EDT) and Soft Robotics is to ascertain the feasibility of using cross-cutting EDT and soft robotics technologies to achieve future NASA mission objectives with mass and power budgets orders of magnitude lower than conventional spacecraft. In this context, the Phase I study focuses on three technological elements: the design of a soft-robotic rover that can operate in extraterrestrial oceans, demonstrating feasibility of electrodynamic tethers for power scavenging in the Europa environment, and utilizing electrolysis to power biomimetic propulsion.

The Phase I results show that a soft robotic, underwater rover has many advantages over a traditional view of autonomous underwater vehicles. Many of these advantages stem from its ability to collapse or expand the body, which carries two key benefits: (i) cost savings in transport and (ii) buoyancy control. Furthermore, this rover's material offers properties that enable it to survive most oceanic conditions, withstand a likely radiation environment, and retard ice formation. The use of these soft robots under water is very attractive because buoyancy enables very large robots without the need for skeletal structures that limit their shape-changing ability. The prime limitation of soft robots for underwater exploration is their nascent state of development, an issue that this study has begun to address and that we hope to continue in Phase II.

The theoretical calculations and experimental investigation on electrodynamic tethers discussed in this report show that their use in saltwater environments is feasible. However, magnetohydrodynamic effects require attention, which will be a priority in Phase II. A possible approach involves magnetic shielding of a portion of the EDT array to generate significant current from imposed alternating magnetic fields. The Phase I experiments show that this approach may enable enough power to be generated for a soft robotic rover of the scale contemplated here. This power is in the range of 1mW to 1W and determines the time required to collect and transmit science data.

The interface between the EDT and rover resembles a fuel cell. This tehnology generates the gases required to power the actuators and recombines these gases, if needed, to extract electricity for several subsystems. For example, there exist science instruments that complement the low mass and low power of our rover and still return substantial new science data. Examples include miniature mass spectrometers, voltammeters, magnetometers, pressure sensors, temperature sensors, and other MEMS and soft sensors. Such a sensor suite can be used to determine chemical-composition data of nutrient particulates in the ocean, magnetic-field specifics, and pressure and temperature gradients.

Designing a soft robotic rover for a mission to the Europan ocean requires a holistic view of the entire mission--for example, accommodating issues of radiation exposure during transit, conditions in the ocean, and conditions during travel through ice. The Phase I study did not concentrate on EDL or passage through the ice, as explained in the Phase I proposal, because JPL and others are already looking into those aspects of a mission. We incorporated these concepts into a general system architecture.

The Europa environment is poorly understood due to the limited scientific data from which to draw conclusions. A mission centered on the proposed soft-rover technology holds promise for answering these conjectures with science data bolstering some definitive answers about the unique Europa environment. Despite these uncertainties, a soft rover has high potential of being capable of surviving in Europa's subsurface ocean environment.

Phase I explored the concept of an eel- or squid-inspired rover. A key conclusion is that a buoyancy-controlled underwater glider may be the best use of a soft actuator's capabilities. The Phase I report summarizes mathematical models of buoyancy and underwater gliding for such a system. Additionally, the Phase I work shows that a rover can use hydrogen fuel for combustion powered hydrojetting. The combination of a buoyancy controlled glider and combustion powered hydrojetting can complement slow, long-duration, underwater exploration with the ability for rapid movements when necessary. As both buoyancy control and hydrojetting use fuel generated from sea water, the in-situ use of resources substantially reduces the launched system mass necessary [1].

These results point to the real utility of both an EDT energy harvesting system and an underwater soft robotic rover. The integration of the two systems via a fuel cell for in-situ resource use motivates further study in a proposed Phase II project.

3   NIAC Concept Evaluation Criteria

The purpose of sending a probe to Europa's subsurface ocean stems from the decadal survey to search for planetary habitats meeting the requirements for earth-like life and new life. To meet this goal, a probe will be designed to explore the subsurface ocean below Europa's ice crust. The niche this rover fills is in cross-cutting low mass and low energy exploration, maximizing the science data returned per tax dollar of the whole mission by substantially reducing system mass.

The goals of this research is to develop a new transportation system that is capable of moving long distances with low energy cost and performing proximity operations at a point of high interest. A majority of the goals for an underwater probe can be achieved at the entry point to the water body as high nutrient transport should occur in this region. Our probe will be capable of performing these subsurface operations, a deep dive, and ocean floor operations. These operations are achieved through exploiting 3 major benefits of using a soft rover—shape change, gas utilization, and material selection.

Key exploitation of shape change is the primary benefit of soft actuators. Buoyancy is an efficient method of transportation that can carry the rover from the subsurface to the depths of Europa, increasing the breadth of all possible science that can be gathered. The rising and falling caused by buoyancy can generate forward motion using soft wings. These soft wings can be made to change shape between large surface areas for low velocity gliding and small surface areas for high velocity gliding. The rate of motion is often dependent upon the "lung capacity" which is quite large for elastomers. Higher velocity shape change resulting from combustion of hydrogen and oxygen gas can be used to power water jets resulting in short bursts of high speed motion. Rapid shape change occurring in sequences can

be used to generate vortex shedding and motion generated based off of pressure differences like an eel or squid.

Key exploitation of fuel utilization provides redundancy in power and multifunctionality. The fuel that will be used to actuate and power the rover comes from the saltwater ocean (in-situ resource utilization). The H_2 and O_2 gas produced by electrolysis first and foremost stores chemical energy to be consumed by the fuel cells for powering guidance, navigation, control, sensors, and communication systems. The H_2 and O_2 gas produced can be used for gradual shape change, such as buoyancy and wing shape change. The H_2 and O_2 gas can be used for high pressure storage for fast actuation of actuators.

Key exploitation of material selection can be used to select composite elastomer combinations that will extend mission life and design robustness to the ocean's uncertainties. Silicone is an ice formation retarding material that will prevent failure due to ice. Silicone is resistant to radiation and only experiences a decrease in material strength. Some elastomers exist that are self-healing, a property that could be exploited to prevent failure due to shearing caused by frazzle ice. Silicone is an inert material that will not significantly interact with the environment. Elastomers can be selected such that they comply with NASA outgassing standards [2]. The silicone material is capable of withstanding current COSPAR decontamination regulations without reducing material properties prior to launch. The silicone material has a low leak rate of H_2 and O_2 gas making it a suitable material for fuel storage.

4   Europa Environment

Understanding the environment is critical to designing any successful robot. The greater the variation in parameters, the more robust the system must be to complete its mission in the unknown environment.

4.1   Internal Composition

There is a high variability in the estimated ice crust thickness dependent upon the method and assumptions used. Predictions range anywhere between 2 and 150 km. Gravity data and spectroscopy of Europa suggest a roughly 150 km thick ice crust and a rocky interior [3]. Analysis of the surface structure ice breakup from surface images suggests the ice thickness is only a few kilometers thick. This image analysis is based off of a comparison between iceberg height versus iceberg width.

The thickness of the Ice on Europa may not be uniform. In fact, the ice may not have a continuous ocean layer, but instead be composed of many smaller lakes bounded by ice that range in starting depths just below the moon's surface from the low predictions of 2 km to the high predictions of 150 km [4].

The depth of the ice shell is calculated to be within 105 and 160Km based off of Galileo gravity measurements, thermodynamic data, high-pressure ices, and meteoritic material. The inner core radius of the moon is predicted to be between 470 to 640 km. The H_2O layer thickness is predicted to be between 115+/-10 km to 135+/-10 km [5].

Due to meteorite impacts and the content of Europa being largely heavier than water, it is likely that there are large rocks somewhere within the ice crust. These rocks would impede the operation of something like the ice drill, VALKYRIE or any other cryobot.

Figure 1: Ice Depth Discrepancies may Indicate Large Lakes of Water in the Ice Crust (Image courtesy of NASA) [4]

4.1.1   Temperature

There are several possibilities for predicting the temperature of the water just below the ice surface. Crude convection modeling indicates an average temperature of 230-240 K. Near surface thermal gradients are expected to be at least 10 K km⁻¹ [3]. This indicates that an ice crust 3Km thick will be at approximately 270 Kelvin and thicker crusts would only mean warmer subsurface temperatures. Penetrative convection from the heat generated in the core and ocean would result in water just milliKelvins above freezing. Maximum density theory suggests that the water exists at its maximum density due to the compressive strength of the ice. This maximum density occurs at a temperature of 3.98°C [6].

4.1.2   Pressure

The water expected to be on Europa is under many km of ice pressurizing the water underneath. Evidence of this pressurization can be observed in the geysers that spray ice and water miles into the air above the planet's surface. Assuming that the depth of the frozen ice is 3 km, interpolation of Figure 3 along the $P_{ex_{crit}}$ indicates that the water pressure is $5 * 10^5$ Pa or roughly 5 atm. If the ice crust is as thick as the 150 km predicted, the maximum pressure of the water could be as high as 150 bar(15 MPa). The maximum the plot indicates is 50km depth resulting in approximately 30 bar of pressure. The nonlinearities in the scale make this pressure difficult to decipher accurately. Calculating the water pressure using the density of ice as $934\,Kg/m^3$ and Europa gravity of $1.315\,m/s^2$ yields a pressure of 36.8bar with a 3 km deep ice sheet assuming all ice rests atop the ocean.

Figure 2:Thermal Vents Diagram (Courtesy of Discovery News)

Figure 3: Water Pressure on Europa vs Ice Crust Depth [38]
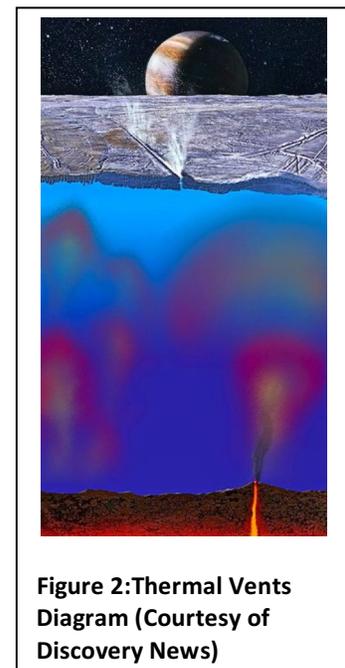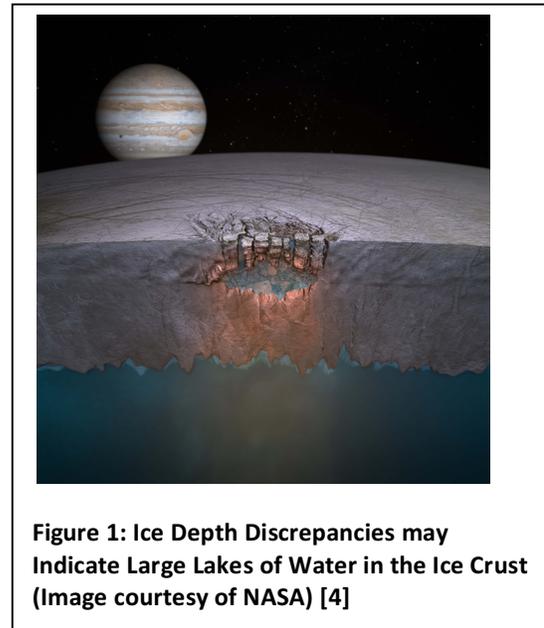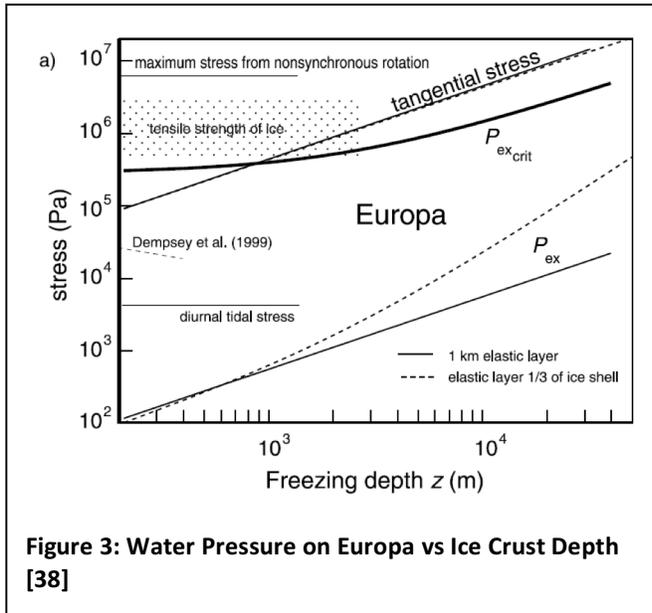
It is important to note that the compressive strength of ice is between 5 and 25 MPa depending on the temperature of the ice (between -10C and -20C) meaning that at some pressure caused by a column of ice, the ice will be continuously fracturing and become an ice water slurry due to phase change [7].

Due to the thermal gradients and tidal forces, it is likely that there are water pockets within the ice itself. It will be critical for the Ice Drill to intelligently determine whether it has encountered a water pocket or the ocean. Additionally, these tidal forces will likely result in loosely packed ice at the bottom of the ice surface. These will exist in a form of slurry that contains ice of varying sizes and constantly freezes and refreezes. It will be important to determine if this region has been encountered and the sizes of the ice chunks encountered. The sizes and frequency of occurrence of these ice chunks is important for optimizing the operation of the rover to be designed. These ice chunks will also have some velocity relative to the Ice crust. This is driven by the prediction of thermal based currents in the water. The resulting ice chunks with velocity present a dangerous scenario for any rover designed as it should be capable of withstanding being crushed between two of these.

4.1.3 Subsurface Currents

The predicted mean radial current speeds are ~3 cm s^{-1} and zonal speeds are upwards of ~250 cm s^{-1}. To give a sense of scale, Gulf currents achieve speeds of ~1 m s^{-1} [8]. This indicates that there are regions of disrupted ice called chaos terrains covering 40% of the satellite's surface.

The chaos regions where the highest transport of fluid occurs is the area of greatest interest as they should contain a representative sample of all chemicals being exchanged at the ice water barrier as well as those being brought up by the thermal vents in Figure 2Figure 2:Thermal Vents Diagram (Courtesy of Discovery News, should they exist. Similarly, the thermal vents and ocean floor are interesting for the same reasons; they represent areas of high nutrient exchange and therefore probability of life.

4.1.4 Proposed NASA Mission: Europa Clipper

In order to refine the planetary properties and behaviors of Europa derived from the Galileo fly by, another probe must be sent with the dedicated mission of collecting data that refine these parameters. NASA has currently proposed a Clipper spacecraft that will flyby Jupiter's moon Europa 45 times in repeated close flybys, seeking the conditions for life by observing the moon.

This satellite will be equipped with an array of sensors. The first of which is a neutral mass spectrometer to analyze materials ejected from Europa's surface for organic materials related to life and for clues to

its ocean composition. Langmuir probes will analyze Jupiter's charged particles that pelt Europa's surface, looking at the possibility of this phenomenon creating oxygen-rich byproducts. Impurity mapping on Europa's surface with a shortwave infrared spectrometer will provide further clues about the ocean's makeup. Magnetometers will determine ocean salinity and depth based on the response to Jupiter's magnetic field. Ice penetrating radar will look for liquid under Europa's Icy shell and determine its thickness. A topographical imager will reveal how geology has shaped Europa's ice and fluid motion in it. A thermal vent imager will detect any active surface features. A reconnaissance camera will survey the surface and look for smooth places suitable for future missions to land on the surface.

While all of these scientific investigations are important, the images of possible landing locations are critical before any landing should be attempted. These images will be used to derive Lander system requirements and identify the optimal landing location.

5   Concept of Operations

Two concepts of operation architectures were considered to deliver the Europa Rover to the surface of Europa. The first proposes to use an orbiter that will deploy a small Lander to surface while the second proposes to use a larger Lander. In both cases, the Lander will house the payload and the drilling mechanism needed to deposit the rover in Europa's ocean. In both architectures, the rover will be stored in the lander with a current packed baseline volume of a 1.25 m long by 20 cm diameter cylinder. This pack volume is based off the current scientific payload bay proposed for the JPL CHIRPS cryo-bot (Zimmerman, 2001). In general, orbiter and Lander architectures will appear better in trade studies at present until an orbiter is sent to Europa so this architecture is the planned mission.

Cornell University
College of Engineering
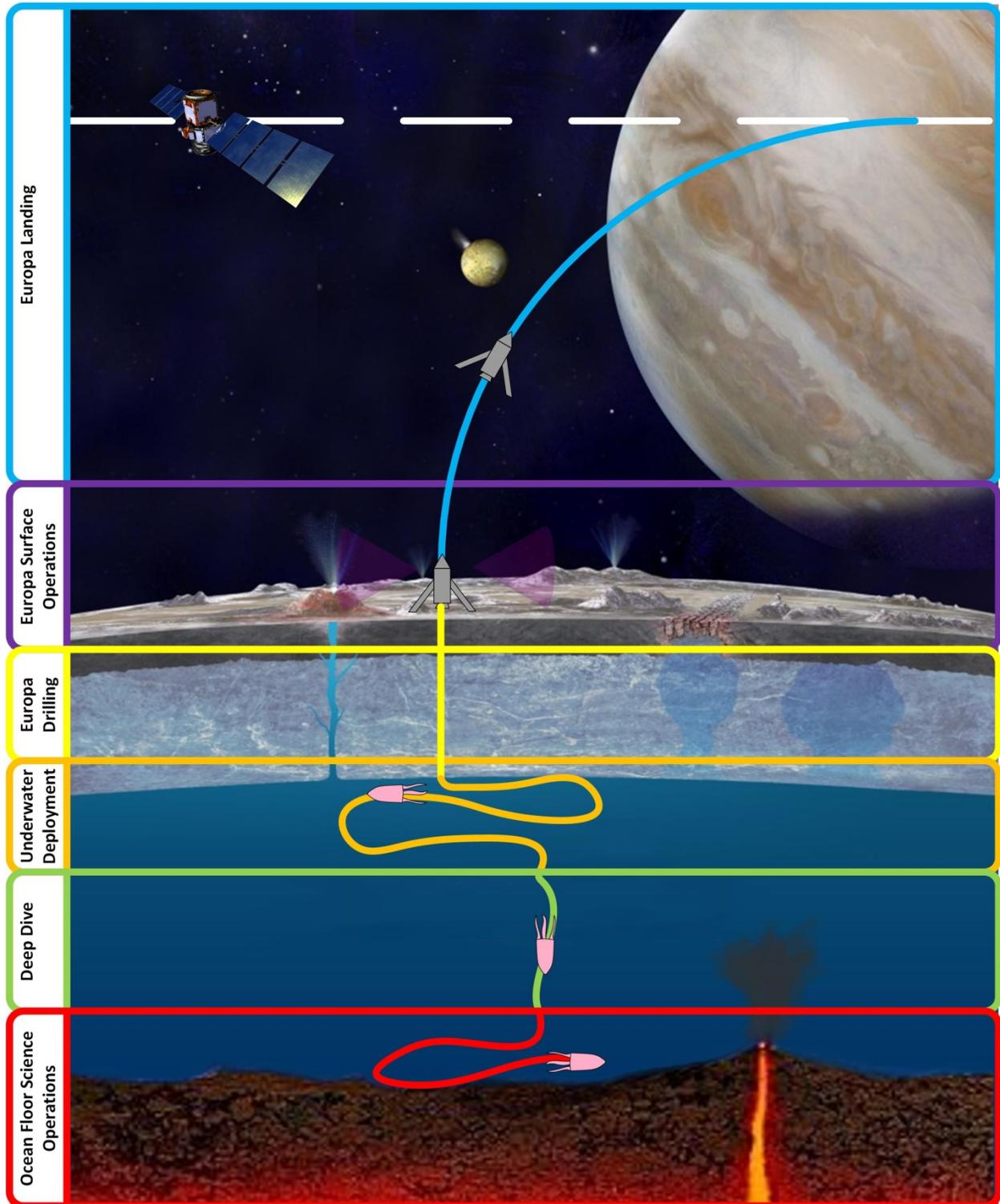
Figure 4: CONOPS for Europa Entry Descent Landing, Surface Operations, Drilling, Underwater Deployment, Deep Dive, and Ocean Floor Operations (parts of image Courtesy of NASA)

The basic modes of operation at Europa begin with the deorbiting of the lander, effectively beginning the entry descent and landing phase of operation where the lander takes control and will autonomously land itself on the surface in the renamed "53 minutes of terror" experience. The lander will then begin deployment of the melt probe and proceed to perform its communication relay and surface science operations. The melt probe will then autonomously drill through the ice for days, performing science operations as it goes until it finally reaches the subsurface ocean. The ice drill will then begin deployment of the rover in development. The ice drill will now act as a communication relay between the rover and lander. The ice drill will also perform any science operations it was designed to perform. The Europa rover will perform subsurface science operations where a majority of the mission critical information is obtained. The rover will then begin its "deep dive" performing science operations along the way. Once the rover reaches the ocean floor, the rover will perform more science operations. Once completed, the rover will rise back to the surface and locate the relative location of the ice drill to relay data back to the surface.

5.1   Orbiter and Lander Architecture

For the orbiter and Lander architecture, the spacecraft will be similar to the Cassini spacecraft delivering the Huygen's probe onto the surface of Saturn's moon Titan. However, because Europa's atmosphere has a negligible density compared to that of Titan's and the Earth's, a more complicated retro rocket propulsion system will be required to perform the entry, landing, and descent (EDL) portion of the mission in place of a parachute. This not only increases mission risk, but the cost, mass, and complexity of the spacecraft as well.

According to unofficial JPL calculations, if a Lander with a mass of 200 kg were added to the Europa Clipper, the mass of the entire spacecraft would more than double due to the extra fuel and EDL retro propulsion stage required. Since the mass of the Europa Clipper is already 5,000 kg, this new architecture would require the heavy lift version of the Space Launch System (SLS) that is estimated to not be complete until the early 2030s. Based off historical data from the Mars Pathfinder and similar missions where a rover is deployed from a Lander, the rover's mass is approximately 5 to 10% of the total mass of the Lander. To be conservative, a maximum estimate value (MEV) for the baseline mass of the Europa Rover is 15 kg [9]. If the probe is not added to the Europa Clipper, an orbiter and Lander architecture with less scientific payloads could be selected to cut down on the mass of the orbiter. If the Europa Clipper does not return data before this mission is carried out, the lack of data from its ice penetrating radar to verify the presence of a global ocean and verify the thickness of the ice crust will increase mission risk.

5.2   Lander Architecture

Mission architecture with just a Lander will require that all communications occur directly between the Lander and Earth. This may result in greater blackout periods and less redundancy compared to a Lander communicating with the Earth or via an orbiter relay.

The second option is to send a Lander without an orbiter. According to [10], with near-future launch vehicles and technologies, the MEV dry mass of the Lander would not exceed 750 kg. This would provide up to 75 kg for the rover, but the reason this mission was dropped in favor of an orbiter is the increased

risk and costs compared to an orbiter. The benefit of both an orbiter and Lander is that if the Lander fails, the orbiter, which is a more well-known system, will be able to provide degraded scientific data to justify the cost and 5-7 years transit time to Jupiter. The orbiter also provides redundancy in communications to the grounds station. Instead of the Lander having to have land with the necessary equipment to communicate with the ground station directly, it can close the link to earth via the orbiter. The orbiter will also have a better field of view compared to the Lander, allowing blackout periods in communication to be minimized.

5.3   Transportation to Subsurface Ocean

5.3.1   Launch Vehicles

The delta V between Earth and Europa is 67,390 m/s [11] and would take 5 years 6 months to get there using a Hohmann transfer orbit although departure and burn times can be adjusted so the spacecraft arrives between 5 and 6 years. This means any underwater rover will require sufficient shielding to survive after that long in the space radiation environment [11].

The basic transportation path from Earth to Europa starts with the launch to space and circularization to orbit. The system will then begin the Hohmann transfer orbit or another alternative maneuver to propel the spacecraft towards Jupiter. The spacecraft will then slow as it enters Jupiter's orbit to enter its gravity well. From here the orbiter may enter orbit of Europa, or swing by in multiple flybys and deposit the Lander during one of these flybys.

Table 1: Launch Vehicles and Orbit Transfer CONOPS (Images Courtesy of NASA)

The baseline SLS configuration, the iCPS upper stage, will be able to deliver 2.9 metric tons to Europa [12].Upper Stage Concept with a single RL-10 B2 engine	
The Large Upper Stage(LUS) with 4 RL10 engines is metric tons to Europa [12].	
The LUS with 2 MB60 engines is capable of sending 8.5 metric tons to Europa [12].	
The LUS with a single J2X engine would be capable of sending 7.1 metric tons to Europa [12].	
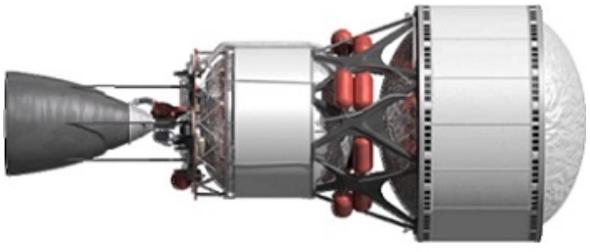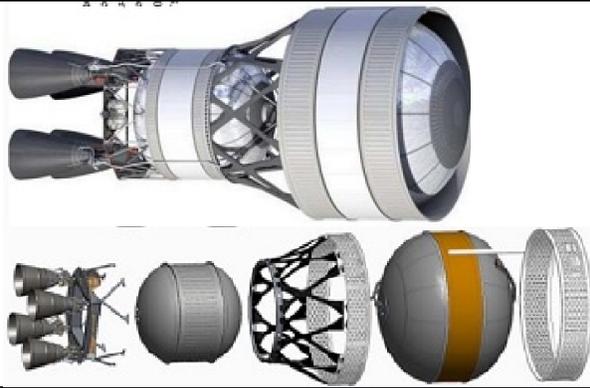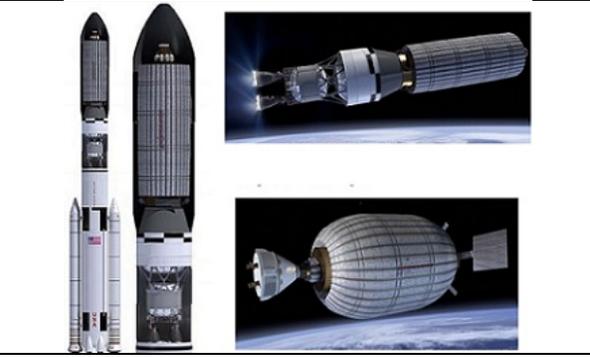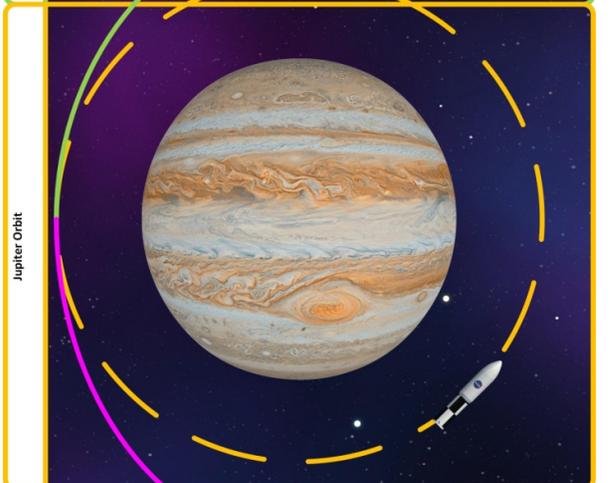
5.3.2   Ice Drill

There are two probes, VALKYRIE and CHIRPS, both known as cryobots and currently are the best known method of breaching Europa's ice crust. Both systems utilize approximately 1 kW of power provided by an RTG to in-take in-situ water, heat it up, and then propel it out to increase heat transfer between the probe and the ice. However, even with this amount of power, the maximum expected drill rate is 2 mhr^{-1}, for a minimum travel time of 200 days through a 10 km sheet of ice. These systems are projected to have a mass of 25-40 kg and prototypes have already been tested, achieving a depth of 10s of meters in glaciers on Earth. While the CHIRPS cryobot could be tethered to explore the polar ice caps of Mars, due to the depth and predicted motion of the ice sheets on Europa, the option of tethering the rover to the lander on the surface for communications and power is infeasible. Instead, they suggest using a series of Beacons dropped periodically during decent to maintain communication between the rover and lander [13].

The proposed cryobot will need to be autonomous as it penetrates through the ice, using sonar to detect rocks and formations in the ice that cannot be melted through. Using directional drilling, a practice common in drilling for oil, the cryobot can maneuver over to something of science interest like a geyser [14].

The VALKYRIE probe will also be equipped with astrobiology sensors that will autonomously make the decision to collect wall core ice samples as it melts through the glacier. The cryobot will also deploy line sensors as it melts through the ice. This will allow for a new method of long-term autonomous glacial monitoring, something that is of interest to the science community [15].

The concept behind the cryobot proposed behind stone aerospace is the use of a long micron-wide fiber-optic cable to transfer up to a theoretical 4.6 megawatts of power from the surface where the thermoelectric generator rests with the Lander to the bottom of the ice crust.

The Ice Drill will also be equipped with its own set of scientific instruments to take measurements as it drills downwards through the ice. These could be anything from ice composition to instruments looking for microbes deposited in the ice using protein fluorescent cytometer [14].
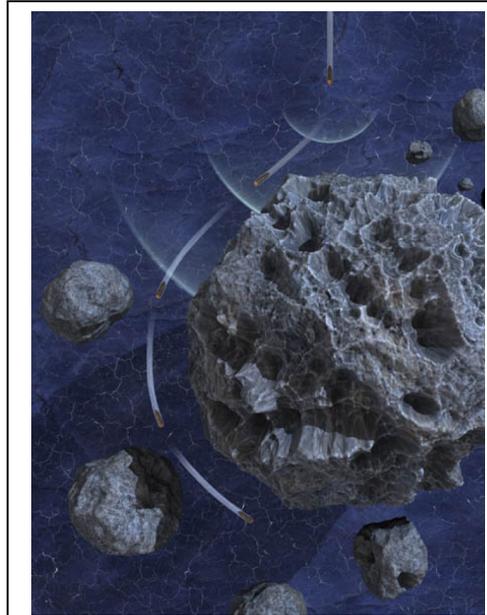
Figure 5: VALKYRIE Impassible object avoidance [15] (Image Courtesy of NASA)

6   Electrodynamic Tethers

6.1   Introduction

EDTs currently have a TRL level of 8 or 9 for Low Earth Orbit (LEO) use, but they have never been used in deep space. The difference between the tethers proposed in this report and those used in past missions are that we are proposing to close the circuit through the saltwater of Europa's Ocean instead of the plasma in the Earth's ionosphere. The majority of tethers deployed in LEO also are used to deorbit or raise the orbit of a spacecraft, while no spacecraft to date has flown with an EDT as its main power source. The closest parallel is the Plasma Motor Generator (PMG) experiment that piggy-backed on the second stage of a Delta II launch vehicle. While its primary purpose was to prove the capabilities of using EDTs to deorbit the second stage, it also generated power using a 500 m insulated tether in LEO [16]. If completing the circuit in saltwater is not feasible, the modest magnetic field experienced at Europa's orbit due to Jupiter and the speed that Europa moves through this magnetic field may make an EDT with a magnetically shielded return cable a viable solution.

Magnetic field perturbations measured during Galileo flybys of Europa are consistent with dipole fields induced by temporal variations of the ambient Jovian magnetosphere. This field behavior is close to what would be expected if the moon was a perfect conductor, which by applying the simple shell model for Europa's conductivity as detailed by Zimmer and Khurana, indicates that there must be regions that have conductivity in excess of 0.06 S/m. Since this kind of conductivity is not possible in ice or silicates, this indicates a body of salt water exists under Europa's ice crust. Combined with the tidal heating that Europa undergoes as it is expands and contracts by Jupiter's gravitational field in its elliptical orbit, the ice crust is expected to be between 2 km and 150 km thick, with 10 km being the most common estimate.

This aquatic environment, whether it be a global ocean or comprised of several underwater "lakes" under the ice crust, are effectively shielded from the harmful radiation of Jupiter's radiation belts and from space debris. If life can exist in the deepest parts of Earth's oceans, then the likelihood of finding life at the ice-water interface of Europa's ice is of interest. The reason to look at this interface is that this is the location where nutrients would be expected to be exchanged between the ocean and the ice crust. However, life may also be present deeper in the ocean depending on the currents and thermal gradient present. The dark red streaks on Europa's surface also may be signs of organic material passing between the ocean through the ice and onto the surface [17]. By sending a rover to the ice-water interface with the necessary payloads to search for life, the mission will satisfy the goal of the most recent Planetary Science Decals Survey to "explore Europa to investigate its habitability and search for life" [18].

From the same Galileo data, the magnetic field that Europa experiences due to Jupiter is between 200-250nT [19]. Jupiter's magnetosphere plasma co-rotates with Jupiter at a mean co-rotational velocity of 118 km s^{-1} at Europa's orbit. However, since Europa is in a retrograde orbit around Jupiter, Europa moves with respect to Jupiter's rotating magnetic field lines at a relative velocity of approximately 102 km s^{-1} [20]. These two parameters are key to determining the best EDT architectures to deploy in Europa's ocean. Also, by crafting a soft-robotic rover that can navigate Europa's ocean biomimetically that is passively powered by an EDT, it is has singular consequences for the possibility of extraterrestrial life based on magnetic energy. While Dirk Schulze-Makuch and Louis N. Irwin assert that this type of

organism is unlikely to exist on the microbial scale, but the possibility of elongated organisms or colonies of organisms, similar that of an EDT used the scavenge power from a magnetic field via the Lorentz force, could be possible [17].

While the use of soft robotics for bioinspired locomotion is a focus of this project, the majority of this work is being developed by Dr. Shepherd's group. Both teams have been in contact to discuss the desired capabilities of rover locomotion, whether it be actively powered by the detonation of hydrogen and oxygen gas created via electrolysis, or if the rover will inflate soft gas vesicles using electrolyzed water to change its shape to navigate the expected currents in Europa's ocean. Using similar locomotion concepts, the inertia of the vehicle may also be used to orient the five EDTs perpendicular to the magnetic field, but this idea must be further explored after determining if an EDT on the order of 10's of meters or 10's of kilometers is needed to generate power within the range of 1 W. Shepherd's team has made great process in learning how to manufacture and actuate soft robotic tentacles and a rover "head" using compressed air. Additionally, Shepherd has demonstrated combustion powered hydrojetting using soft actuators and hydrogen gas generated via water electrolysis.

To design the EDT, the methodology outlined in the Tethers in Space Hand Book was used to estimate the amount of power a given tether could produce in Europa's ocean. Unlike past tethers that harvest power via the Lorentz force by completing the circuit in Earth's ionosphere in LEO, our tether could complete the circuit when immersed in saltwater or a shielded cable. The questions that must be answered first is if it is possible to generate current via an EDT in saltwater or a shielded cable. One concern is that a bare tether in saltwater would be effectively grounded along the entire length of the tether, thus inhibiting it from gaining the necessary electromotive force along its length via the Lorentz force to generate power. If a sheathed tether is used with two bare ends in saltwater, the next question is what is the optimal exposed area for power generation? For the equivalent space system, a hollow cathode system is used to emit a dense cloud of plasma at either end by ionizing a gas [21]. While this process consumes a small amount of energy, it greatly increases the plasma density at either end of the tether to lower the effective resistance of the tether system. This process will be discussed in detail in the analysis section when the data from the Plasma Motor Generator (PMG) experiment is used to validate the predicted power of the aquatic EDT in the Analysis Section. The PMG experiment also shows that the effective resistance of plasma is approximately three to four orders of magnitude lower than that of a column of saltwater, which was an unexpected result that will be verified through testing.

While all proposed mechanisms to drill through a 10 km ice crust propose use a radioisotope thermal generator (RTG) with a power output on the order of 0.6-0.8 kW, the inclusion of an EDT that is able to power the rover after reaching the ice-water interface is a significant enabling technology to explore other moons in our solar system that orbit plant's with strong magnetic fields. Unlike solar power, an EDT will generate continuous power as long as it is oriented perpendicular to the magnetic field and is independent of its distance to the sun. It also avoids the use of an RTG fueled by plutonium, which is currently scarce and expensive to handle. The unique properties of an EDT immersed in saltwater may enable the creation of architectures that utilize multiple tethers in various directions that are close together.

6.2   For Europa's Oceans

While past EDTs utilize the plasma of the ionosphere in LEO, the tether for the Europa Rover proposes to use the conductivity of saltwater to complete the circuit. The initial hypothesis was that the conductivity of saltwater would be much lower than that of plasma, thus enabling the tether to be more effective than in space. However, preliminary calculations based of the conductance of saltwater show this not to be the case. When comparing the resistance of a 500 m tether immersed in saltwater to the 500 m tether of the Plasma Motor Generator (PMG) experiment, the resistance of saltwater was found to be three to four orders of magnitude larger than that of the plasma when in full sunlight. The result is that a carbon fiber tether on the order of 75 km would be needed in order to provide a little over 1.13 watts. This number also assumes that the entire length of the tether is aligned perpendicular to that of Jupiter's magnetic field.

While silver and copper wire have much lower resistances than that of carbon fiber, the main driver for the length of the tether is the high resistance of saltwater. This led to the investigation of a magnetically shielded return line to complete the circuit using Mu-Metal iron-alloy foil. Since Mu-Metal as thin as 0.002" is capable of attenuating an external magnetic field in excess of a factor of 1,000, this tether architecture appears to have the capability of generating 1 watt with tether that is 100's of meters long. Since Jupiter's magnetic field is only 200-250 nT compared to the 18,000 nT provided by Earth's magnetic field in LEO, redirecting the magnetic field with Mu-Metal or another iron alloy with a high magnetic permeability is feasible. Currently 0.002"-0.020" Mu-Metal is used to create rooms that are isolated from Earth's magnetic field, which ranges from 0.25 to 0.65 gauss on the surface of the Earth.

The challenge with a tether on the order of 100's of kilometers rather than 100's of meters is that it is difficult to complete the circuit in the ocean. If a tether this long was suggested, it would make sense to deploy the tether as the rover descends through the ice crust. However, based off a feasibility study performed by JPL for a communication and power tether to connect the CHRIPS cryobot to a lander on Europa, the mass of the tether and the amount of shielding required to stop it from being sheared from the moving ice crust would make it infeasible. The mass of the 75 km tether, even if it was assumed to have the density of carbon fiber tow, would be several 100 to 1,000's of kilograms, making this option infeasible without modification. The predicted mass for a variety of carbon fiber, copper, and aluminum tethers are show in Table 2. The other downside of carbon fiber tow is that its electrical conductivity is on the order of 10e-5, which is three orders of magnitude lower than silver. If we assume that graphene wire will be able in the near future, a conductivity of 10e-8 could be used.

Table 2: Power generation for EDTs of different material with saltwater closing the circuit

Material	Density (kg/m^3)	No. of Tethers	Length (m)	Diameter (m)	Volume (m^3)	Mass (kg)	Power (W)
Carbon Fiber Tow	1790	1	1000	1.60E-03	2.01E-03	3.60	4.88E-05
Carbon Fiber Tow	1790	5	1000	1.60E-03	2.01E-03	18.00	2.44E-04
Carbon Fiber Tow	1790	1	5000	1.60E-03	1.01E-02	18.00	2.44E-04
Carbon Fiber Tow	1790	1	10000	1.60E-03	2.01E-02	35.99	4.88E-04
Carbon Fiber Tow	1790	1	4000	4.00E-03	5.03E-02	89.98	2.19E-03
Copper	8940	1	1000	1.60E-03	2.01E-03	17.97	2.56E-04
Carbon Fiber Tow	1790	1	75000	1.00E-02	5.89E+00	10543.97	1.13
Carbon Fiber Tow	1790	75	1000	1.00E-03	5.89E-02	7907.98	0.1125
Carbon Fiber Tow	1790	1	75000	1.00E-02	5.89E+00	10543.97	1.13
Carbon Fiber Tow	1790	75	1000	1.00E-03	5.89E-02	7907.98	0.1125

The path between both ends of the tether can be reduced by creating a parallel tether architecture where the effective 75km length is achieved via 75 1km tethers. In space, the ability to place two tethers next to one another is limited by the Debeye length, which defines how far the electrostatic effects of a source persist. When an EDT produces a current, if it is approximated as an infinite wire, it produces a magnetic field according (1:

$$B = \frac{\mu_o I}{2\pi r} \qquad (1)$$

Where B is the magnetic field generated by the wire, μ_o is the magnetic permeability of the conductor, I is the current flowing through the wire, and r is the radius of the wire. The formula to calculate the Debye length in an electrolyte, which is assumed to be ocean sea water, is given in (2:

$$\kappa^{-1} = \sqrt{\frac{\varepsilon_r \varepsilon_o k_B T}{2 N_A e^2 I}} \qquad (2)$$

Where I is the Ionic strength of the electrolyte, ε_o is the permittivity of free space, ε_r is the dielectric constant of the electrolyte, T is the temperature of the electrolyte in Kelvin, N_A is Avogadro's number, and e is the charge of an electron. By substituting the values for saltwater,κ^{-1}, which is the symbol used to denote the Debye length in an electrolyte, is approximately 1.23e-8 m. This means that if two "active" wires that are scavenging power from Jupiter's magnetic field are placed next to one another separated by a thin layer of saltwater, the magnetic fields they produce will not affect one another. A similar calculation for the Debye length in the ionosphere and magnetosphere of earth is on the order of 10e-3 and 10e2 respectively, which may make parallel tethers bundled close together not an option [22].

Whether placing two tethers right next to one another when immersed in saltwater effectively doubles the current will have to be tested using the set ups discussed in Section 5 in the future.

Figure 6: Magnetically shielded conducting core with 12 "active" EDT wires in parallel to scavenge power
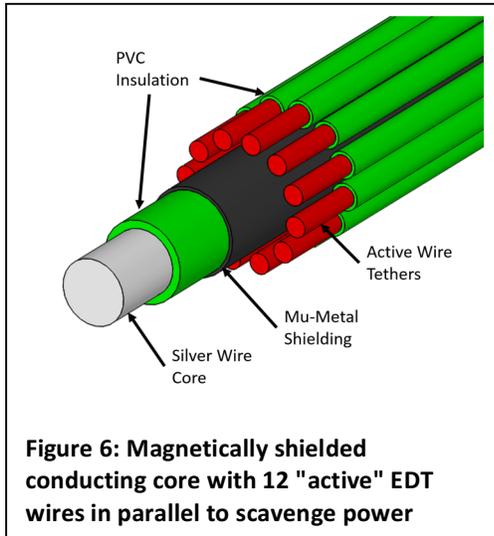
One potential design chosen to analyze as an example in detail is shown in Figure 6. This EDT architecture combines the possibility of 12 parallel EDTs to shorten the overall length of the system and the concept of circumventing the high resistance of the saltwater by using a silver return cable that is shielded from Jupiter's magnetic field by a thin Mu-Metal foil. In order for the Mu-Metal to effectively shield the center core, it must not make contact with the center core conductor or the conductor of the active tether wires. This is why a flexible PVC insulator was chosen to cover all the conducting wires. This insulator also helps prevent arcing between wires if they build up a large enough difference in potential, but this effect must be analyzed in greater detail when sizing the thickness of the insulation material. Other polymers may be advantageous, as PVC becomes brittle at temperatures expected near the surface of Europa despite being corrosion resistant. Due to its use in common household electrical wire insulation, it will be used for experimentation. This design is predicted to produce upwards of 1 watt with a 100 meter length with the core wire being 18 gage silver and the outer "active" wires being 28 gage silver.

6.3 Analysis of Current through Water

Because the conductivity of an electrolytic solution (seawater, for instance) depends on the concentration of the ionic species, it is valuable to know how the ionic strength of the water might affect the various aspects of performance of an EDT underwater.

Current generation: Following Ohm's law, the effective resistance of a path of current through water directly relates to the magnitude of the current generated, as

$$R = \frac{U}{i}$$ **(3)**

Where R is the resistance (Ω, "ohms"), U is the potential difference (V, "Volts") and *i* is the current (A, "Amperes"). Conductance G (S, Siemens) is then defined as the reciprocal of the resistance:

$$G = \frac{1}{R} = \frac{\kappa A}{l}$$ **(4)**

And κ is the conductivity (S m^{-1}), A is the cross-sectional area of the electrodes (m^2; i.e., the effective area available for conducting electrons through liquid), and l is the distance between electrodes (m). κ is directly proportional to the molar concentration of the electrolytic solution, c

Therefore, the Ionic strength of a solution is related to the molar concentration by (5:

$$I = \frac{1}{2}\sum_{i=1}^{n} c_i z_i{}^2 \qquad \textbf{(5)}$$

Where z_i is the charge number of the ion, and the sum is taken over all ions in the solution.

Using these equations, we determine that the resistance of the water is inversely proportional to the ionic strength of the electrolyte, and so a strong electrolyte will give us a larger current generated.

$$i = \frac{U\kappa A}{l} \propto \frac{UIA}{l} \qquad \textbf{(6)}$$

Debye Length: the magnitude of the ionic strength of the solution is also related to the Debye length, and so this could be a useful variable (though because the Debye length is already so small, our system is not very sensitive to the ionic strength here).

6.4   Magnetically Shielded Tether Analysis

To calculate the electromotive force produced in a single EDT, the equation for the Lorentz force can be arranged to yield (7 as stated in the *Tethers in Space Handbook*:

$$V_{emf} = \vec{v}\times\vec{B} \cdot \vec{L} \qquad \textbf{(7)}$$

where $\vec{v}$ is the velocity of the tether with respect to the magnetic field, $\vec{B}$ is the magnetic field, and $\vec{v}\times\vec{B}$ is equivalent to the electric field generated along the length of the tether, which is then projected onto the length of tether, $\vec{L}$, via the dot product. The result is V_{emf} , which is the electromotive force within the wire. (7 can be re-written into scalar form using the definitions of a cross product and dot product in (8:

$$V_{emf} = v\text{B L}\sin(\theta)\,cos(\phi) \qquad \textbf{(8)}$$

Where θ is the angle between the velocity vector of the tether and the magnetic field vector, and ϕ is the angle between the direction of the electrical field and the length of the tether. To estimate the

current and power generated by a single EDT in saltwater, the total system resistance, R_{sys}, is equivalent to (9:

$$R_{sys} = R_T + R_W + R_{load} \qquad \textbf{(9)}$$

Where R_T is the resistance of the tether, R_W the resistance of the saltwater, and R_{load} is the resistance of the rover in ohms. When solving for R_W, the resistance of saltwater is on the order of 1e3 ohms for an insulated 10 m tether and is heavily dependent of the contact area present at the ends of the tether. This prediction will be verified by experiment. The result is a low current, which requires a tether on the order of 75 km, as stated in [21], to produce power on the order of 1W using (13.

To avoid the high resistance of saltwater, an EDT comprised of several "active" tethers in parallel with a single magnetically shielded tether core, as discussed in Section 3.6, may be feasible. The concept of magnetic shielding utilizes a material with a high magnetic permeability, μ, to redirect the magnetic field lines around the conductor one wishes to shield. Mu-Metal, which is an iron alloy, is such a material and is used to create zero gauss chambers in lab spaces and shield electrical components from external magnetic shields. When exposed to an external magnetic field in H_o, the magnetic flux density in the shield material, B, is found using (10:

$$(10)$$
$$B = (1.25DH_o)/t$$

Where D is the diameter of the shield in inches, t is the thickness of the shield in inches, and both B and H_o are given in Gauss. B is the strength of the magnetic field that needs to be re-directed within the shield itself. By using the B-H Flux Density versus Magnetizing Force curve given in Figure 7for Mu-Metal, the magnetic permeability of the material, μ, can be approximated via the diagonals on the graph. The magnetic field attenuation, A, provided by the shield is then given in (11, where t is the thickness of the shield and D is the diameter of the wire to be shielded.

$$A = (\mu * t)/D \qquad \textbf{(11)}$$

Since H_o is equivalent to 200 nT-250 nT, which is the magnetic field of Jupiter at Europa, a 0.002" thick shield with a diameter equivalent to 18 gauge wire, provides an attenuation on the order of 1e3, which essentially reduces the field strength in the core wire to zero. This will provide a low resistance return path for the active tethers that is independent of the resistance of saltwater. However, in Figure 6, a gap must be provided between each active tether to allow saltwater to surround each tether. If the prediction that the Debye length is on the order of 1e-8m is true from (2, this will ensure the active

tethers will not interfere with one another.

Figure 7: D.C. Permeability of Mu-Metal magnetic shielding materials versus the magnetizing force, H [23]

Figure 8: Circuit diagram for magnetically shielded wire core with n active tethers in parallel
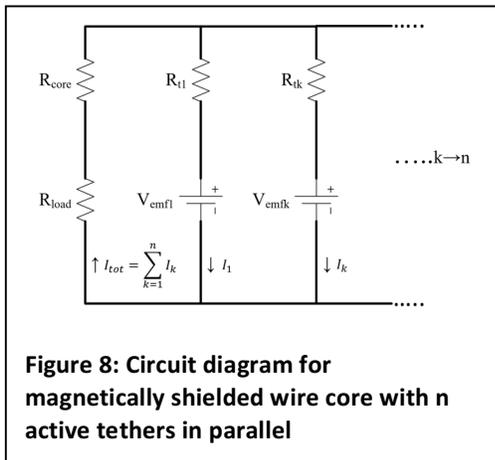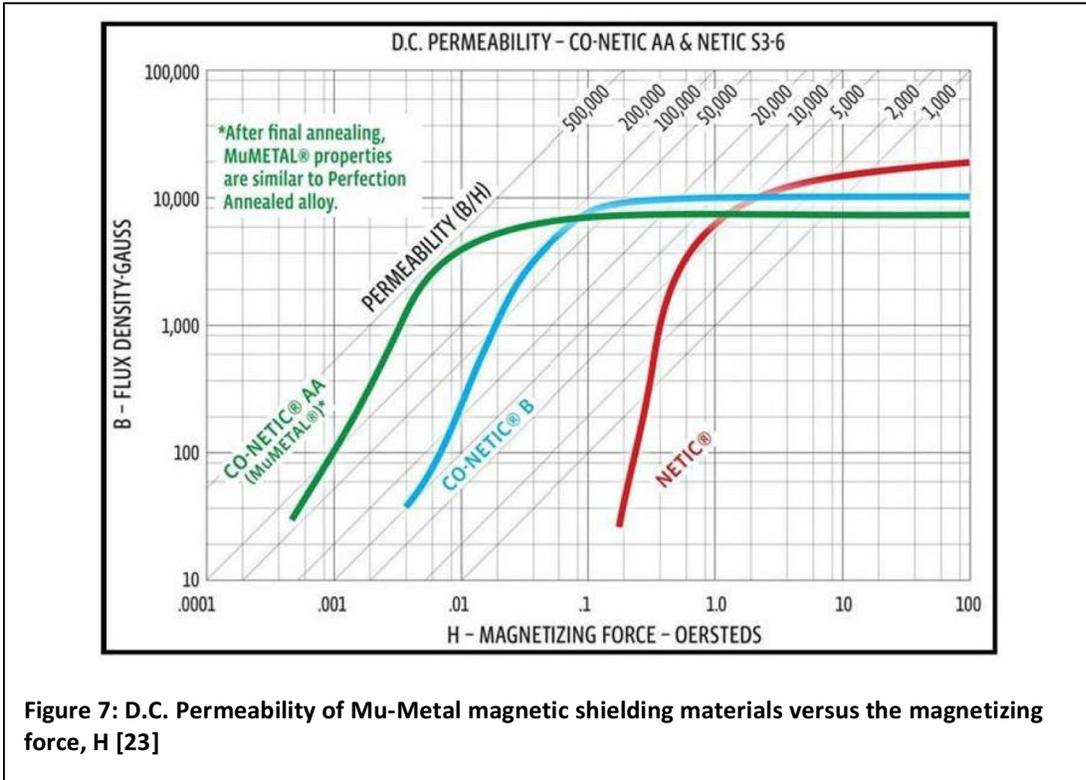
Another benefit derived from using n active tethers in parallel around a magnetically shielded core is that the resistance of each active tether, R_t , is in parallel with the resistance of the core, R_{core}, and the resistance of the rover, R_{load}. This circuit diagram for this system is depicted in (9.

Assuming each active tether produces an identical V_{emf} according to (8, by using Kirchoff's Law, the expression for the total current passing through the rover, I_{tot} , is given by (12:

$$I_{tot} = \frac{V_{emf}}{R_T + n(R_{core} + R_{load})}$$ **(12)**

The power generated by the tether can then be found by (13:

$$P = I_{tot}V_{emf}$$ **(13)**

The calculations for the magnetically shielded core with 12 active tethers (n=12) is shown in Table 3 and Table 4. The linear density of this tether is estimated to be 5226.2 kg/m^3, which results in a 100 m

tether predicted to generate 1.16 watts of power with a mass of approximately 2.31 kg. For this calculation, the resistance of the rover is assumed to be negligible. Further research will be needed to confirm the validity of this analysis and to test the ability of the Mu-Metal foil to attenuate a 250nT field. However, the ability of a 0.002" thick Mu-Metal shield to attenuate the 0.25-0.65 G electric field of the Earth by a factor of 1000, shows this option to be promising [23].

Table 3: Calculations for magnetically shielded core wire with 12 tethers in parallel

Magnetically Shielded Tether					
L (m)	Number of Tethers	Resistance of Load (Ω)			
100	12	0			
18 Gauge Wire					
D (mm)	Density of Silver (kg/m^3)	V (m^3)	M (kg)	Resistivity of Silver (Ωm)	Resistance of Return Wire (Ω)
1.024	10490	8.229E-05	0.863	1.59E-08	1.93
28 Gauge Wire					
D (mm)	Density of Silver (kg/m^3)	V (m^3)	M (kg)	Resistivity of Silver (Ωm)	Resistance of Active Wire (Ω)
0.320	10490	9.653E-05	1.013	1.59E-08	19.77
18 Gauge Insulation					
t (mm)	D_o (mm)	D_I (mm)	Density of PVC (kg/m^3)	V (m^3)	M (kg)
0.0762	1.176	1.024	1100	2.633E-05	0.0290
28 Gauge Insulation					
t (mm)	D_o (mm)	D_I (mm)	Density of PVC (kg/m^3)	V (m^3)	M (kg)
0.127	0.574	0.320	1100	2.140E-04	0.235
Mu-Metal Shielding					
t (mm)	D_o (mm)	D_I (mm)	Density of PVC (kg/m^3)	V (m^3)	M (kg)
0.0508	1.278	1.176	8700	1.958E-05	0.170
Total Mass (kg)	**Total Volume (m^3)**	**Total Density (kg/m^3)**	**Total Diameter (mm)**		
2.310639456	4.388E-04	5266.2	2.426		

Table 4: Power calculations using the magnetically shielded tether defined in Table 3 and the calculations presented in the Tethers in Space Handbook

Magnetically Shielded Tether Power Generation		
Variable	**Units**	**Value**
v_rel	m/s	1.02E+05
B	T	2.00E-07
L	m/s	100
Θ	Degrees	90
Φ	Degrees	0
V_emf	V	2.04
R_tether	Ω	42.95
I_tether	A	0.57
P_tether	W	1.16

6.5   Bare Tether Experiments

A quick, initial setup was first used to determine the possibility of an EDT being used in this environment. As such, this model aimed to reflect the best possible conditions for current generation underwater. Because water salinity and temperature were widely variable in our understanding of Europa's environment, we chose to create test setups that would offer constant geometric properties (wire length, distance from magnetic field, etc.) and that would allow us to easily change the water properties to their extrema by draining and filling our setup with different water preparations through a port on one of the bulkheads. Due to the current's dependency on the Ionic strength of the solution, it would be best to test solutions with the highest possible concentrations. After proving the concept is possible, according to the *Galileo* observations, we can determine the most effective setup is a solution with conductivity between 0.02 and 0.06 S/m [19]. For reference, the typical conductivity of ocean water on Earth is 5 S/m, the conductivity of drinking water is in the range of 0.005 – 0.05 mS/m, and the conductivity of distilled water would approach zero [24].

In order to simulate the physics for the EDT, our wire 'tether' was placed within a hollow PVC cylinder of 1 inch inner-diameter, and suspended in the center of the cylinder by four acrylic cutouts with small holes in their centers, and a 'spoke' design to allow water to freely flow between the sections of the test setup. The wire is centered in the cylinder in order to keep it perpendicular to the magnetic field, and to allow us to pass magnets across the length of the cylinder from any angular orientation of the subscale mockup. The wires
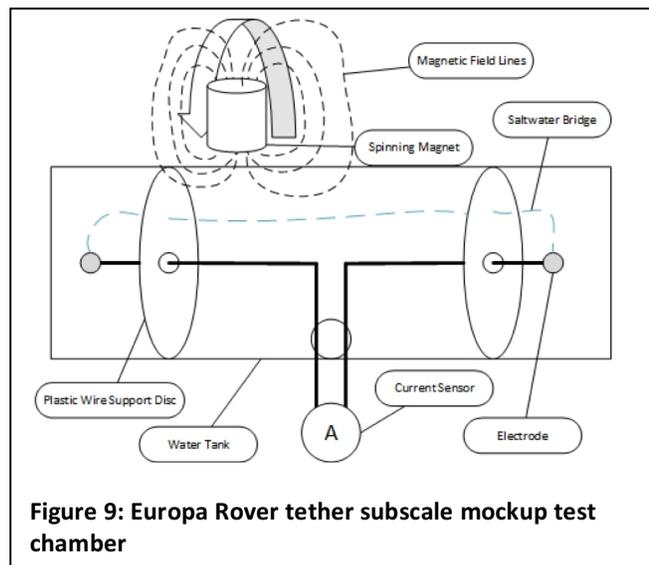
Figure 9: Europa Rover tether subscale mockup test chamber

meet at the center of the cylinder where they will then exit through a small hole and are connected to a multimeter in order to measure the current and voltage generated. We have chosen standard copper wire for its high conductivity and abundance, which will make it a good candidate for this test.

Following the production of the test setup, a single cylindrical magnet was attached to the end of a power drill and spun perpendicular to the wire setup, alternating between north and south poles as it spun through its radial center. Due to limits in measurement capabilities of AC power, we were unable to measure beyond the milliamp range in current and the millivolt range in voltage. However, initial experiments of this test setup yielded occasional readings of 1mA, signaling that current generation through the electrolyte may be possible and warranting further study after obtaining more sensitive measurement devices.

This testing also revealed the difficulty in measuring the current generated solely as a result of the EDT, as the circuit setup does not allow any one place to measure current independently. The current will always be dependent on two unknowns; the voltage generated by the EDT, and the resistance of the water, both of which are under examination and cannot be assumed to be known.

6.6   Magnetically Shielded Tether

Though having shown that we may be able to develop a current using the electrolytic solution, the magnetic field required in order to do this would be thousands of times stronger than that of Europa's field, and still would result in extremely large lengths of tether in order to be able to generate even 1 mW of power. As previously shown for a magnetically shielded tether, there will be no current generated in half of the loop, and only the active tether which is outside of the shielding will experience the EMF associated with the magnetic field. This vastly reduces the predicted resistance (~10 kOhm to ~10 mOhm) compared to the saltwater tether, and will provide a greater current for the same voltage yielding greater power per length of tether. The numbers expressed in Tables 5 and 6 for initial estimates of this type of tether are promising – nearly 1 W of power for 1000 m of total tether length, and so it became a priority to pursue a test case for how predictable this type of power generation actually is.

To test the numerical model, a set of Mu-Metal magnetic shielding was acquired, and a 2ft long sleeve of shielding was used to test the physical model (part #1/4" SSC-250). The maximum field strength for the Mu-Metal shielding to not experience saturation was found to be 70 Gauss, or .007 Tesla, according to the equations in the magnetically shielded tether analysis. This provides the information for selecting the magnets for experimentation, and magnets were ordered such that their magnetic field strength would yield 70 Gauss at a distance of 1.25 inches.

The magnets were set into a PVC pipe with their poles aligned and facing radially out from the PVC pipe, spaced .8" away from one another in order to fit 24 of them within an 18 inch section, to be centered over the Mu-Metal sleeve assembly; in order to avoid end effects, we did not align magnets over the whole length of the shielding, but centered the magnet assembly with 3 inches free on either side.

There is some readily available documentation on how to solve for the magnetic field at any location in space due to two point charges, yet it has been hard to find analytical equations of a magnetic field of a physical magnet, where the magnetic field strength is a property of magnet dimensions. This has made it difficult to fully realize the strength of the magnetic field at any location along the path of the wire, but with the help of K&J

Figure 10: Magnetically Shielded Tether Test Setup

Magnetics field strength calculators we were able to solve for the field strength of each magnet at various key points along the length of the wire. However, due to the vector addition of the magnetic fields from each magnet, the perpendicular field across the wire will be influenced by several magnets at a time. The result is an average magnetic field of about 100 Gauss at a distance of 1.5 inches – this is unfortunately entering the realm of saturation.

The magnet tube assembly is rotated at ~3000RPM above a tank with a Mu-metal sleeve assembly being suspended in water. The sleeve is suspended within the water by extending a length of string across the filled tank and tensioning it, to keep the sleeve as taut as possible.

An alternating current is generated in this setup – this happens as the magnetic poles drive the positive and the negative maxima while rotating. The calculations for the voltage potential generated in a length of wire due to magnetic fields are all considered for DC considerations, but a quick conversion from AC to DC is acceptable here to consider the root mean square voltage (Vrms) that is the equivalent DC voltage;

$$V_{RMS} = .7071 V_{max} \qquad \textbf{(14)}$$

The max voltage is calculated using the maximum value obtained from the magnetic field at the distance, according to the calculations presented in the magnetically shielded tether analysis.

With a single tether, then, attached to a 1.5 Ohm resistor, we should theoretically expect data as in Table 5 and Table 6.

Table 5: Magnetically Shielded Tether Properties

Magnetically Shielded Tether						
L (m)	Number of Tethers	Resistance of Load (Ω)				
0.5	1	1.5				
20 Gauge Wire						
D (mm)	Density of Copper (kg/m^3)	V (m^3)	M (kg)		Resistivity of Copper (Ωm)	Resistance of Return Wire (Ω)
0.812	10490	2.58924E-07	0.00271611		1.70E-08	0.016414097
20 Gauge Wire						
D (mm)	Density of Copper (kg/m^3)	V (m^3)	M (kg)		Resistivity of Silver (Ωm)	Resistance of Active Wire (Ω)
0.812	10490	2.58924E-07	0.00271611		1.70E-08	0.016414097

Table 6: Magnetically Shielded Tether Power Generation using the parameters in Table 5

Magnetically Shielded Tether Power Generation		
Variable	Units	Value
v_rel	m/s	1.5000
B	T	0.0100
L	M	0.5
Θ	Degrees	90
Φ	Degrees	0
V_emf	V	0.00530
R_tether	Ω	1.53283
I_tether	A	0.00346
P_tether	W	0.00002

From testing of the experimental setup using the Mu-Metal sleeve, and under various resistance values, the results presented in Table 7 were found.

Table 7: Mu-Metal Sleeve Testing

Resistor (Ω)	Current (mA)	Voltage (mV)
0	3	0
1.5	1	4.2
4.7	0	4.4
10	0	4.6
100	0	4.9
1000	0	5.3

These results show that the theoretical values for voltage vary on average only about 10% from the measured values. The expected current, however, does not match the results obtained from experimentation – rather, the real current with a 1.5 Ohm resistor is much more representative of the current expected with no additional resistances outside of the wire resistance.

In order to further examine our ability to predict the current, we tested the same setup using an additional tether (theoretically doubling the current) and then up to five tethers (theoretically quintupling the current), as shown in Table 8.

Table 8: EDT Current Generation Dependency on number of Tethers

2 Tethers			5 Tethers		
Resistor (Ω)	Current (mA)	Voltage (mV)	Resistor (Ω)	Current (mA)	Voltage (mV)
0	3	0	**0**	3	0
1.5	1	4.4	**1.5**	2	4.5
4.7	0	4.5	**4.7**	1	4.6
10	0	4.6	**10**	0	4.8
100	0	4.7	**100**	0	5.2
1000	0	4.7	**1000**	0	6

As we saw before, the voltage is remaining relatively constant across different resistances, but the current is changing as if it worked the same as the single tether EDT – though there is a slightest increase in the five tether regime, but this could be due to measurement error.

6.7   Conclusion

While the results of the experimentation will convince that there is some validation of the EDT for use in energy scavenging on Europa, further testing must be done to truly understand the physics and reliability of the models used in predicting the power output of such a device. It is apparent that the model, as is, does not capture full understanding of the phenomena at work and must be revisited with focus on the generation of current due to the magnetic fields across the whole length of many wires, and how we should really expect the resulting power to look. The initial estimates of the potential power, especially in that of the magnetically shielded tether, are very promising – and it seems that from initial experiments that our model consistently predicts a power 3 times greater than what we're finding. Even with this, a simple scaling of tether length to accommodate this error would only mean

needing a shielded tether of 3,000 m in length, being still within the realm of possibility in a subsurface Europa rover.

The insulated tether experiment shows that a current can be produced within a traditional EDT by completing the circuit through an electrolyte, but further testing must be done in order to confirm the predictability of models to fit the resistance of the water and the voltage generated by the magnetic field. Unfortunately, due to measurement sensitivity constraints, the data collected is very rough and does not provide significant insight into either the current generated or the resistance of the water – both of which are major unknowns within the experiment. In addition, this experiment was complete with very limited physical conditions which should be expanded to really check understanding of the phenomena at play; for instance, the length of the tether utilized here is potentially 1/10000 of the length that would be required on Europa by initial calculations, and it could be beneficial to test the model across a large spatial dimension.

The magnetically shielded tether loop model also needs to be expanded to include a spatial dimension, and this is especially relevant due to the discrepancies between the expected addition of current for each tether loop completed and what was actually found – it may be that we can no longer expect to add many tethers around a single core tether. Errors in our understanding here could be resulting from a few options; misunderstanding of the way that the magnetic fields produce an EMF within a whole length of wire at once; ways that current generated can add together within a circuit as created; Debye length considerations, as perhaps the current generated in one wire is negatively influencing the current in others. In addition, the magnetic field strength is not confirmed at the location given, but only provided through analytical means, and this affects the accuracy of the model in unpredictable ways.

7   Europa Rover Science Instruments

7.1   Mass Spectrometers

Mass spectrometers are used to measure the mass and relative concentrations of atoms and molecules. Generally, mass spectrometers are quite large and consume large quantities of power. Miniature mass spectrometers are a newer technological development that is not currently used on spacecraft. The largest problem with mini mass spectrometers is the requirement to manually separate samples. This includes the sample collection, extraction, pre-separation, and other special treatments highly dependent upon the nature of the samples collected. Scientists have been working with microfluidics to perform chip based sample preparation using solvents. The samples our rover will be measuring will all be located in convenient water solution already so additional solvents do not need to be brought.

The primary drawback of decreasing mass analysis instrument size results in mass resolution degradation as smaller volumes result in loss of resolution mostly through smaller trapping capacity. The reduction in mass and size of a mass spectrometer has a cascading effect on the other systems required.
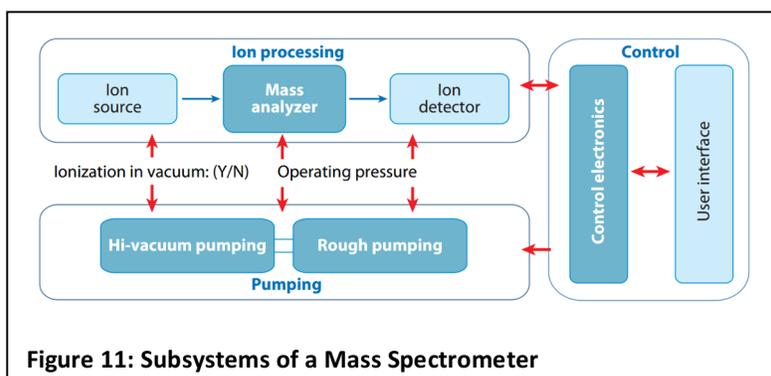
Figure 11: Subsystems of a Mass Spectrometer

There are several drawbacks and advantages of miniaturizing spectrometers. The primary drawback is the reduction in mass resolution caused by shrinking the mass analyzer, but some of this can be mitigated by higher end electromagnets with undistorted geometries. A key advantage is that smaller spectrometer trap volumes imply allowed operation at magnitudes of higher pressure, reducing the pump requirements and size linearly with size decrease. Another advantage is the decrease in control

Table 9: Various Mass Spectrometer Spectral Resolution, Mass, and Energy Consumption [39]

Systems	Self-sustainable portable systems						Portable systems without rough pumping	
	Mini 10/Mini 11 (3, 4)	ChemCube™ (115)	Guardion-7™ (5)	Suitcase TOF (9)	Griffin 600™ (116)	Ion-camera (117)	Palm-portable MS (52)	HAPSITE® (74)
Developer	Purdue University	Microsaic Systems	Torion Technologies	Johns Hopkins Applied Physics Lab	Griffin Analytical Technologies, Inc.	OI Analytical	Samyang Chemical Co.	Inficon
Weight	10 kg /4 kg	14 kg	11 kg	N/A	15 kg	18 kg	1.5 kg	18 kg
Power	70 W/30 W	50 W	75 W	N/A	N/A	75 W	5 W	<150 W
Mass analyzer	Rectilinear ion trap	Quadrupole mass filter	Toroidal ion trap	TOF	Cylindrical ion trap	Mattauch–Herzog sector	Cylindrical ion trap	Quadrupole mass filter
MS/MS	Yes	No	Yes	No	Yes	No	No	No
Sampling/ ionization	MIMS, direct leak, GDEI, APCI, ESI, DESI, LTP	SPME, EI	SPME, mini GCEI	MALDI	SPME, MIMS EI	Direct gas leak EI	Pulsed gas leak EI	GCEI
Mass range/ resolution	m/z 700, R = 700; m/z 1500, R = 750	m/z 600, R = 400	m/z 500, R = 500	m/z 70,000, R = 70	m/z 425, R = 400	m/z 300, R = 300	m/z 300, R = 150	m/z 300, R = 300

system requirements due to the lower forces necessary to keep the same magnetic field strengths.

When analyzing complex mixtures, mass spectrometry minimizes chemical noise and allows acquisition of information about the chemical structure. The important question to ask about mass spectrometry is what spatial resolution is required to satisfactorily categorize each chemical element we expect we could find in this environment? What false categorizations could occur? Can we accept the drawbacks of a miniature mass spectrometer? The benefits of different size mass spectrometers can be observed in Table 9. In power requirement calculation, analysis times are <1s [25].

7.1.1   Chromatography

Chromatography is the separation of two fluids or particles in a fluid via absorption. This is extremely advantageous for our rover as Europa is expected to provide the water solvent for the water based life sought. The one catch is the non-specific chemicals being searched for. It is desirable to know the quantity and presence of each different element in the water and it is not yet known exactly what those could be or the quantities they exist in. Therefore, before chromatography is further investigated, it is crucial that the chemicals most expected to be found, and strongest indicators of life be included as chromatography becomes very specific to the chemicals being measured as the absorption process can quickly become a filtering process.

There are many different possible separation techniques. These include ultrafiltration (UF), size-exclusion chromatography (SEC), ion-exchange chromatography (IEC), reversed-phase chromatography (RPC), ion-pairing (IP) RPC, and capillary electrophoresis (CE). CE comprises several separation modes: free-zone electrophoresis (CZE) and isoelectric focusing (IEF). The questions that have arisen are what are the optimal filtration methods? What filtration systems should be considered? Further investigation can occur through research into the subject. Chapter 22 of this book [26] discusses the positives and negatives of the different species separation techniques.

Of these techniques mentioned, capillary electrophoresis (CE), provides efficient separation and is excellent for supplementing liquid chromatography methods. Analysis time is comparatively short and separation efficiency is high. CE exerts only minor disturbances on organometallic complexes.

7.2   Voltammetry & Polarography

Voltammetry is a type of potentiodynamic electrochemical measurement. The basic operation of voltammetry is essentially the measurement of the rate of deposition of a material on the anode or cathode based on the changes in current with voltage. The idea is that the change in current against potential can be used to analyze redox reactions and oxidation reactions. This also allows the concentration and nature of the ions in the water to be measured. This will allow us to analyze Europa's water for its composition and concentration [27]. These sensors could be simple low mass electrodes on the outside of the rover capable of verifying mass spectrometer and chemical analysis.

7.3   Sonar

A rover mounted sonar system is impractical due to the shear mass, size, and power required for larger sonar systems capable of sensing over long distances. While smaller, lower power, and compact sonar systems do exist, they are only capable of measuring depth to a few meters, only useful for proximity detection and could be used to determine if the rover is stuck. There are some interesting pieces of information that can be obtained by a single underwater acoustic sensor. This could lead to ice geology findings based on the cracking rate of the ice.

In studying the correlation between sonar range and resolution, it was found that longer range sonar and higher resolutions resulted in larger numbers of transmitters and receivers needed. This correlates to higher system masses, higher power requirements, higher data output, and higher processing power required.

7.4   Camera

The primary stakeholders of NASA are the American public, then the government, who is advised by the scientists interested in this mission. The scientific value of a camera on the surface of Mars, where daylight occurs is obvious as rapid surveying can take place. Under 2Km to 150Km of ice more than a million miles from the sun, a camera is virtually useless. There are exactly four things that the soft robot rover may take a picture of: (i) The melt probe it has been released from (ii) The ice formations beneath the surface (iii) The ocean floor (iv) Floating Ice chunks and particulate. We believe there are additional benefits to having an on-board camera and will consider it an essential component of payload.

7.5   Magnetometer

This would be good because we should not have any magnets aboard our vehicle that would interfere with magnetic field readings of Jupiter's magnetic field through Europa. This can provide a good plot of the magnetic field under Europa's surface. The mass spectrometer should have a magnet in it that may be characterizable to not significantly affect results.

7.6   Tactile Soft Robot Sensors

Soft Robots that undergo large shape deformation require feedback control. Sensing techniques using stretchable capacitors have high precision and sensitivity over large strains and pressures. PI Shepherd has used these stretchable capacitors to detect compressive forces of ~2N and internal pressurization as low as 10kPa, well below the pressures to be used in the rover actuators. During the course of the Phase I program, we determined that the chemistry of these sensors is not compatible with the harsh conditions of space travel. We have developed a new chemistry, based on carbon nanotubes, that allows us to fabricate stretchable sensors that are robust to the expected conditions during spaceflight and oceanic conditions.

Both external and internal strains can be detected using inks imbedded in the soft robotic rover head and tentacles, indicating when the device is actuated or has contacted something giving the soft robotic rover external feedback for little additional mass. Imagine the entire exterior of the rover being covered in miniature sensors measuring strain, temperature, pressure, and performing voltammetry.

8   Flexible Electronics

To complement the flexibility of the soft robotics, there exists a thriving field of flexible electronics. Presently, these exist as the printing of conductive inks onto glass and thin paper substrates. These substrates are capable of being layered and can store large quantities of energy in printed super capacitors. Work at the Marshall Space Flight Center is looking into the inks that make printing these circuits possible, but there are endless possibilities and the mass of the circuitry could be substantially reduced and distributed around the rover's actuators' inextensible layers. Dow Corning is producing a new product in large quantities called willow glass, an ultra thin flexible piece of glass and are actively looking for applications. Printing circuits on this substrate and putting it in the rover could be one of those applications as these will produce ultra low-mass circuitry.

9   Electrolysis

A majority of the power that the rover receives will go directly into electrolyzing water present on Europa. Electrolysis operates by dissociating hydrogen and oxygen molecules in water into their respective gasses. This process is as simple as applying a voltage to an anode and cathode this results in current across a reversible fuel cell that is correlated to the proton exchange across the membrane. In general, the Horizon Fuel cells we use operate between 0 and 5 volts and 0 to 2 amps depending on the disassociation rate, pressures of the gasses, and amount of fuel available.

It is important to note that the rover does not bring any fuel with it since all the fuel will be generated on Europa with the help of the EDT. The H_2 and O_2 gas that is generated is used for numerous applications. First, the gas that is produced has higher chemical energy potential than water. This can be harvest in two ways. The first is by pumping the H_2 and O_2 gas into the Fuel Cells, creating a voltage and current output. This power can be used to charge a battery, super capacitors, or run electronics. The second energy release is through combustion reactions. This operates based off of the rapid release of thermal energy and expansion of the resulting H_2O vapor. This second method can be used to produce rapid shape change in soft actuators resulting in high forces, and rapid displacements of fluid resulting in propulsion. Another application of the produced gas is to inflate an actuator based on pressure differentials. The final use of this gas is for density change and water displacement resulting in buoyant forces acting on the system.

One possible problem that will need to be overcome if this rover is to come to fruition is the saturation of the proton exchange membrane (PEM) with salt ions. The only partially direct indication of the ocean's content is a spectral analysis of waterplumes ejecting from Europa's surface, indicating the ejected water contains salt. Electrolyzing with fuel cells in a saltwater environment results in the gradual saturation of the PEM membrane in Na and Cl ions; gradually ceasing all electrolysis. There are methods by which the salt ions can be removed such as boiling the membrane in freshwater but a proactive approach that passively solves the problem will be far more effective and merge easily with the rover's numerous passive abilities. Using more advanced membranes such as borohydride can reduce the rate at which salt ions accumulate as they do not have as high of an affinity. Similarly, salt ion filters have advanced a long way making saltwater desalination a feasible option for a future space mission by using reverse osmosis to desalinate the fluid.

For testing purposes in actuating soft machines, mini PEM horizon fuel cells were tested in the lab. These fuel cells will operate for up to 8 hours in a brine solution before the electrolysis essentially stops as shown in Figure 12.

Further tests were performed. These indicated the hydrogen side of the membrane will generate pressures up to 33 psi and the oxygen side of the membrane will reach pressures up to 7.5 psi. Hydrogen pressures above 33 psi result in failure of the membrane and hydrogen gas leaks. This failure is largely due to cheap manufacturing of the fuel cell. Oxygen pressures above 7 psi results in permeation of the PEM membrane and oxygen leakage through water inlet channels. This essentially stopped the fuel cell from producing any more oxygen or hydrogen. It is important to note that these fuel cells can get into a state where they cannot produce gas. In the short term, this can be mitigated by flushing the oxygen side of the membrane with water and restarting. An alternative is to wait for the hydrogen and oxygen to recombine into water.

Figure 12: Fuel Cell Degradation vs Time

The 33 psi generated is more than sufficient to power the soft actuators, better designed fuel cells and membranes result in higher hydrogen pressures and possibly oxygen pressures. There is much research in this area and even some going on at Cornell. It is necessary to note that the pressures experienced are all pressure differentials; meaning the pressure inside will be 33 psi higher than the external pressure. This could result in a substantial number of moles of gas if the ice crust is 150 km thick and the water pressure is 150 bar.

Hydrogen and oxygen should always be stored separately from one another. Aside from them being highly reactive, they will also gradually recombine over time meaning an oxyhydrogen mixture will revert into water given enough time. This time scale is orders of magnitude larger than the power generation rate and therefore fuel generation rate. It is best practice to store hydrogen and oxygen separately from one another.

A proton exchange membrane could even be implemented in the skin of the rover. The PEM is relatively flexible and should act just like an inextensible layer of our actuators. This integration into the skin would be interesting to study into the future.

10 Silicone Material

10.1 Ice Retarding Properties

The primary concern regarding the formation of ice is the added mass to the system hindering motion, the possibility of the rover freezing to the ice crust. There is also concern that the ice formed could result in shearing of the silicone. The good news is that silicone naturally retards the formation of ice on its surface. Ice formation on uncoated polished aluminum at -15°C is approximately 5 seconds [28]. Hydrophobic and superhydrophobic coatings can be prepared using silicone rubber doped with titania, ceria, and carbon black nanopowders that drastically lengthen this ice formation time on aluminum surfaces. Our rover will be essentially made of this ice formation retarding material.

10.2 Gas Permeability

A major concern with the storage of hydrogen and oxygen is that hydrogen leaks out of every container it is stored in. Assuming a 1.107L spherical balloon of thickness 1cm filled with oxyhydrogen gas, at a ratio of $2H_2$ to $1O_2$ molecule, at 0.5atm above external pressure, will have a leak rate of $2.635 * 10^{-14} \, cc/second$. The leak rate of a pure H_2 storage under comparable conditions is $2.6776 * 10^{-14} \, cc/second$. The leak rate of O_2 storage under comparable conditions is $2.6055 * 10^{-14} \, cc/second$. For comparison, storing hydrogen gas in a copper tank has the same rough order of magnitude of leak rate as silicone under comparable circumstances. Similarly, storing hydrogen gas in a steel tank has an order of magnitude higher leak rate than silicone. This is because the size of a hydrogen particle is substantially smaller than the crystalline structure of the copper and steel.

Comparison of gas permeability with natural rubber=100 for reference (25°C)

Material			H₂	O₂	N₂	CO₂	Air
Natural rubber	P x 10⁸cc-cm cm²-sec-atm		37.4	17.7	6.1	99.6	—
			100	100	100	100	100
Silicone rubber			1070	2200	3300	1600	2700
Butyl rubber (isobutene 98, isoprene 2)			15	56	5	4	48
Polybutadiene (emulsified)			86	82	80	105	81
Nitrile	Acrylonitrile content	20%	51	35	31	48	33
		27%	32	17	13	24	15
		32%	24	10	7.5	14	8.5
Teflon®			46	44	43	19	—
Polyethylene d=0.926			15	11	9	8	—
Polypropylene			23	7	9	4	—
Polyvinyl chloride			6	2	2	1	—

Water vapor permeability of plastic films

Material	Water vapor permeability*
Silicone rubber	15.5-51.8
PVA	0.04-40.0
Ethylcellulose	21.5
Polyethylene	0.05-4.85
Polytetrafluoroethylene (PTFE)	2.94
Polycarbonate	1.0
Nylon	0.32-0.63

$$\ast \text{ Permeability} \quad \frac{(cm^3 \text{ gas})(cm \text{ thickness}) \times 10^{-7}}{(sec) \, (cm^2) \, (cmHg\Delta p)}$$

Figure 13: Permeability of gasses through silicone rubber and water vapor permeability [29]

Note that elongating a storage container will change the maximum leak rate as the surface area of the vessel increases. The current calculation shows optimal geometry.
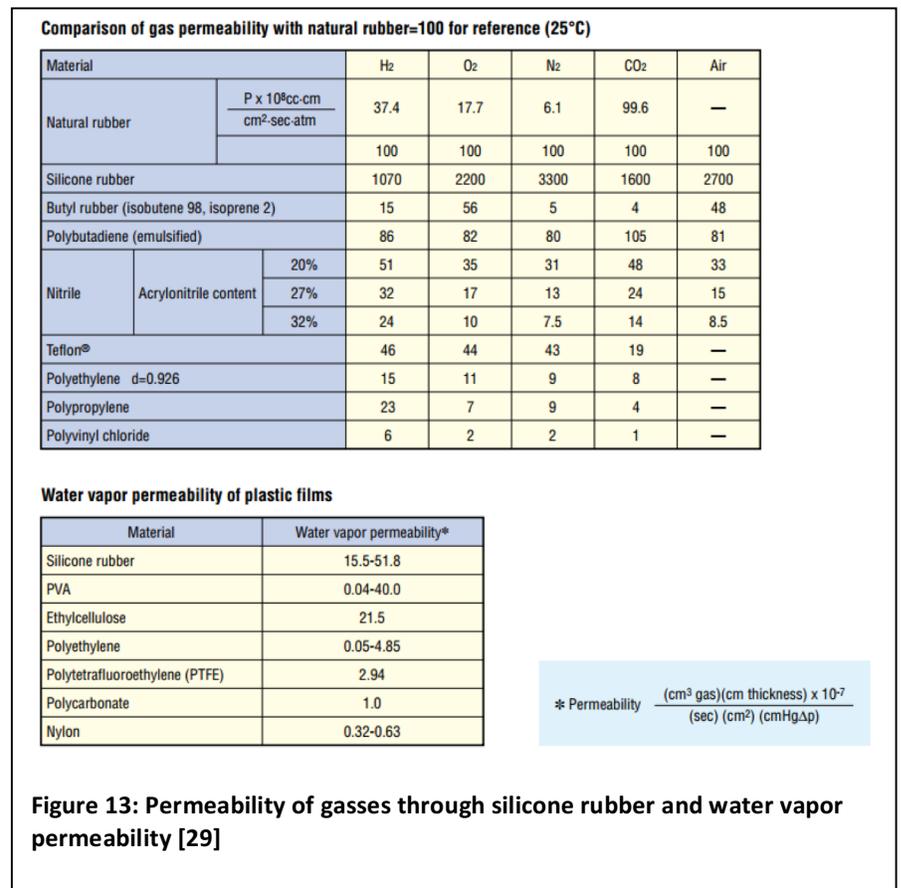
10.3   Corrosion

Silicone rubber is chemically inert and does not corrode other materials [29]. Exposure of a silicone test piece was immersed in artificial urine for 14 days and no changes in mechanical properties or internal structure were observed.

10.4   Radiation

Radiation is a problem for a Europa mission given the long 5 to 7 year trip through the unprotected space environment that is continually exposed to galactic cosmic radiation. Radiation analysis has been performed for manned missions to the Jupiter system that reports radiation doses on the order of 120 cSv (cumulative sieverts) [30]. The equivalent in gamma ray dosage is 12000 rad. Based on the material properties in Figure 14 and the calculated gamma ray dosage, the material properties should not decrease as they are orders of magnitude lower than the radiation dose. The radiation emitted by Jupiter is significantly higher than transit space. This would imply that time spent in orbit of the planet would have a substantially higher radiation dosage per day and this analysis may not be valid.

It is important to note that common Silicone Rubber (dimethyl silicone rubber) has no significantly different radiation resistance than other silicone rubbers.

Once the rover is inserted into the liquid ocean, there should be minimal radiation that afflicts the rover as it will be under kilometers of natural radiation shielding from the ice crust.

The effects of silicone exposure to radiation leads to weakened material properties, lowering maximum tensile strength and lowering maximum strain. This reduction in strength can be dealt with by using thicker parts (the strain limitation cannot be overcome). The thicker parts also help with the containment of hydrogen and oxygen.

Figure 14: Gamma Ray Radiation resistance of rubbers and effect of radiation dose on elongation at break, hardness, and tensile strength [29]
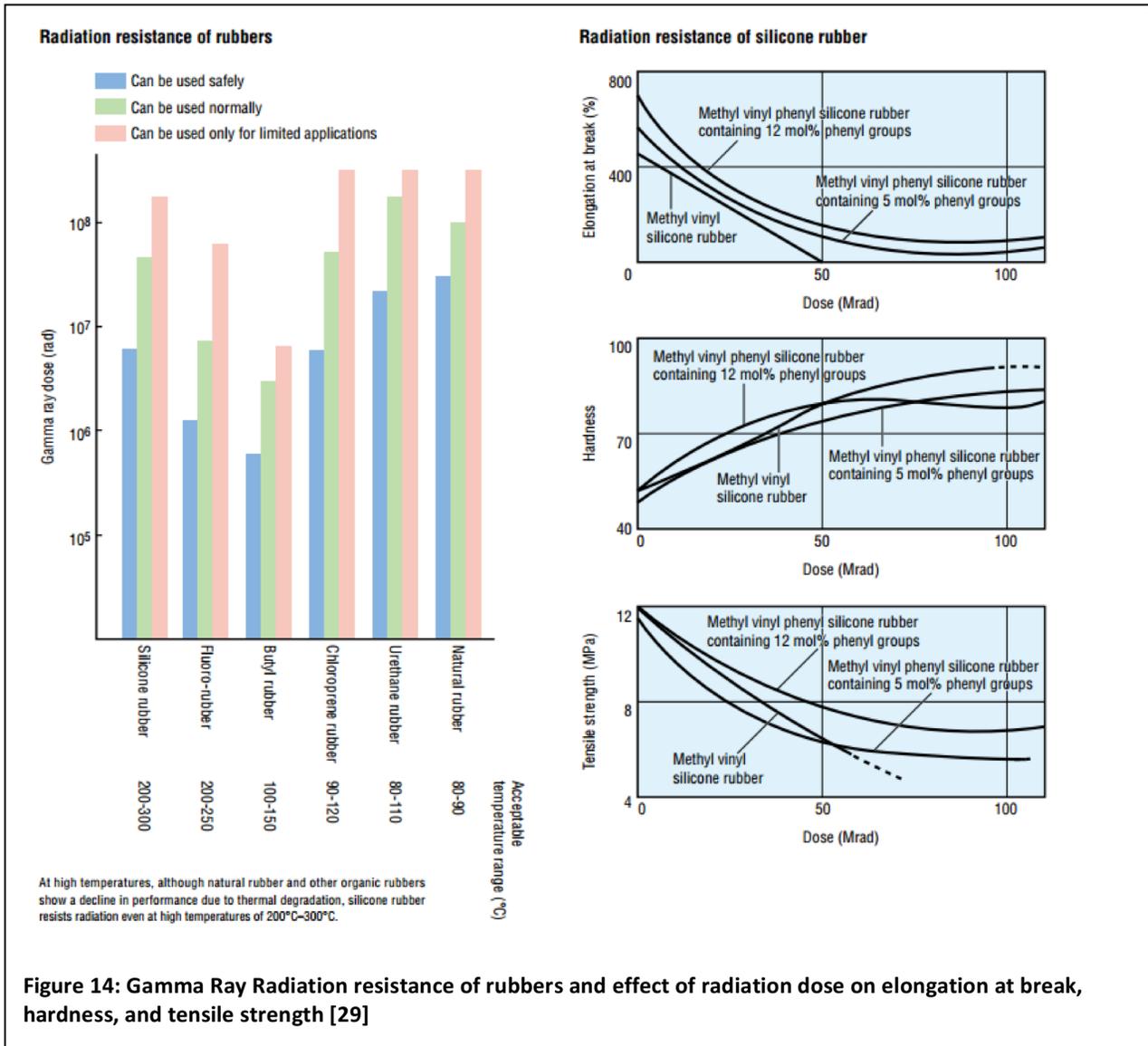
10.5 Outgassing

While the rover should be sealed in some form of capsule for delivery to Europa on the melt probe, all of the materials on the Europa Rover should comply with NASA's outgassing standard of less than .5% of material mass reduction. There exist numerous silicones and rubbers in the NASA outgassing database presently. These silicones and rubbers are mainly used as washers, O-rings, and seals. Our silicone rubber will need to be tested, but it is so chemically stable that it is unlikely to outgas but material scientists have been surprised in the past.

10.6 Temperature Dependent Properties

There should be a note that the material properties of most elastomers change greatly with temperature compared to most other space materials. The minimum temperature, based on current scientific analysis, our probe could be expected to reach is 230K. The subsurface ocean should be warmer near the 273K range. The highest temperature the rover will reach should occur during decontamination at 111.7°C.

Figure 15: Material Properties of Silicone Rubbers and other Rubbers at High Temperatures [29]

Figure 16: Low Temperature Properties of Silicone Rubber

At the high end of the temperature spectrum during decontamination, the maximum temperature of the rover will not exceed 160°C where the material will begin to change material properties based on Figure 15. At the lower end of the spectrum, 230K or -43°C the modulus of rigidity significantly increases for general purpose silicone rubber increases from 1 MPa to 10 MPa from Figure 16. A few degrees cooler and it will be as tough as 150 MPa. Silicones do exist that can operate at substantially cooler temperatures with lower modulus of elasticity whereas other rubbers become stiffer at even higher temperatures.

10.6.1 Decontamination

When NASA missions leave Earth to explore another planet, they must meet internationally accepted standards of planetary protection established by the Committee on Space Research (COSPAR). These standards vary based on the goal of the spacecraft and often define how it is assembled in a clean room on Earth. After the Mars Exploration Rovers were sterilized at the standard 80°C for 15 minutes, the left over organism diversity was observed and found spore-forming bacteria as the dominant fraction of microorganisms left over, specifically Tersicoccus phoenicis. A newer method of sterilization has been presented at the European Astrobiology meeting using ionized gas at low pressure that achieves full spore inactivation within 5 minutes. While this new method is gaining acceptance, it will be some time before the scientific community is wholly convinced. The only two accepted methods at the moment are dry heat; cooking the surface to 111.7°C, or hydrogen peroxide. Both of these techniques can damage

advanced materials but silicone material properties are unaffected by both of these techniques due to its molecular stability and high melting point [31].

Since the probe will make direct contact with a body of water, new Planetary Protection measures must be taken to ensure that exploration is conducted in a way that avoids "the introduction of extraterrestrial matter" to Europa in accordance with Article IX of the 1967 Outer Space Treaty [32].

10.7 Manufacturing Process

The manufacturing process used to create the ellipsoid expansion bladder used in the combustion experiments and buoyancy experiments was produced by centrifugal casting. The general process for manufacturing with our silicones is to spray the ellipsoid mold with mold release, mix equal parts of Ecoflex 10 part A and part B, pour into our ellipsoid mold being sure to coat the walls, and set in the rotational caster for approximately 2 hours. After 2 hours has passed, the mold is placed in an oven at an elevated temperature for 30 minutes. This process creates a completely sealed ellipsoid mold.

The rotation rate of the slow side of the rotational caster is 0.77 rotations per second. With an approximate 2:1 spin rate, the other axis rotates at 1.54 rotations per second. This differential in the spin rate allows the ellipsoid mold to become evenly coated as long as the mold's centroid is located about the center of rotation. If the mold is not centered about the center of rotation, the resulting bladder will become misshapen. This uneven coating can also occur if the inside of both halves of the mold are not lightly brushed with the Ecoflex prior to placing in the caster. An additional step that is often implemented is holding the mold upside down in the rotational caster for 30 seconds before starting. This needs to occur because a significant amount of time elapses between when the silicone is poured and when it is mounted in the rotational caster. This is not time sensitive because the silicones are curing, but because sitting too long on one side prior to casting causes pooling that cannot be evenly distributed by the rotational caster.

11 Mobility Research

11.1 Crawling and Undulating

Italian researchers have replicated the motions of an octopus tentacle using single and double servo motion. The tentacle is powered using servos and cables that work to expand and contract the limb using the silicone material as a compression string. In 100 mm distance motion, the robot achieves average speed comparable to 3.9 mm s^{-1} with maximum speeds of 4.35 cm s^{-1} in single servo operation and 5.55 cm s^{-1} in double servo operation [33]. This kind of motion could be useful for navigation at the ocean floor or the underside of the ice crust.

11.2 Vortex Shedding

Studies have found that eels and jellyfish are the most efficient swimmers. Researchers at the University of South Florida have found that eels are so efficient in their motion because they use both low and high pressures to propel themselves forward [34].

11.3 Poroelastic Foams

Figure 17: Schematic of pneumatic actuator subsystem of lamprey and figures demonstrating reliable actuation over millions of cycles [37]
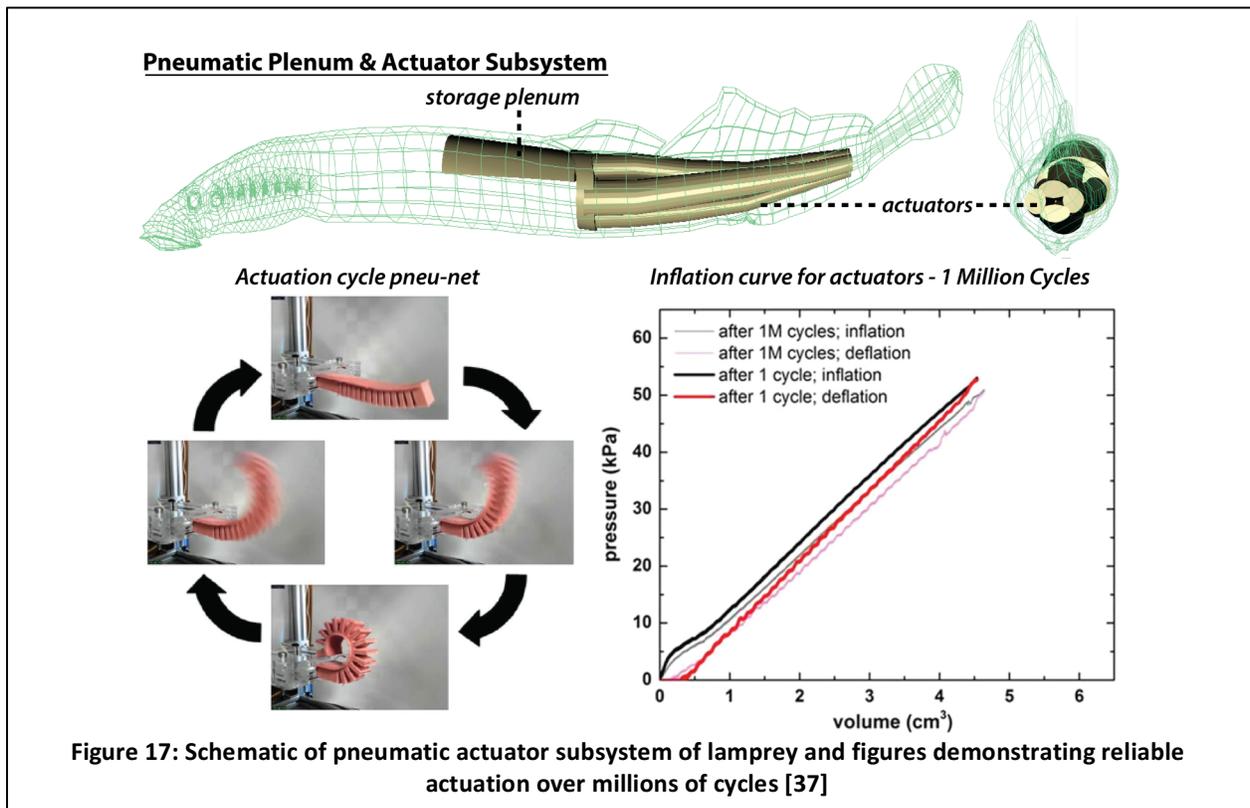
During the Phase I study we went beyond theoretical calculations and tested first prototypes of several subsystems of the robotic lamprey: (i) pneumatic steering/gas storage, (ii) water electrolyzer, (iii) gas storage/combustion hydrojet, (iv) sensory and light emitting skins. In addition, we performed theoretical calculations for the electrodynamic tether. After this study, we believe even more strongly that this approach has actual potential for entirely new and useful rovers, as well as new power generation systems.
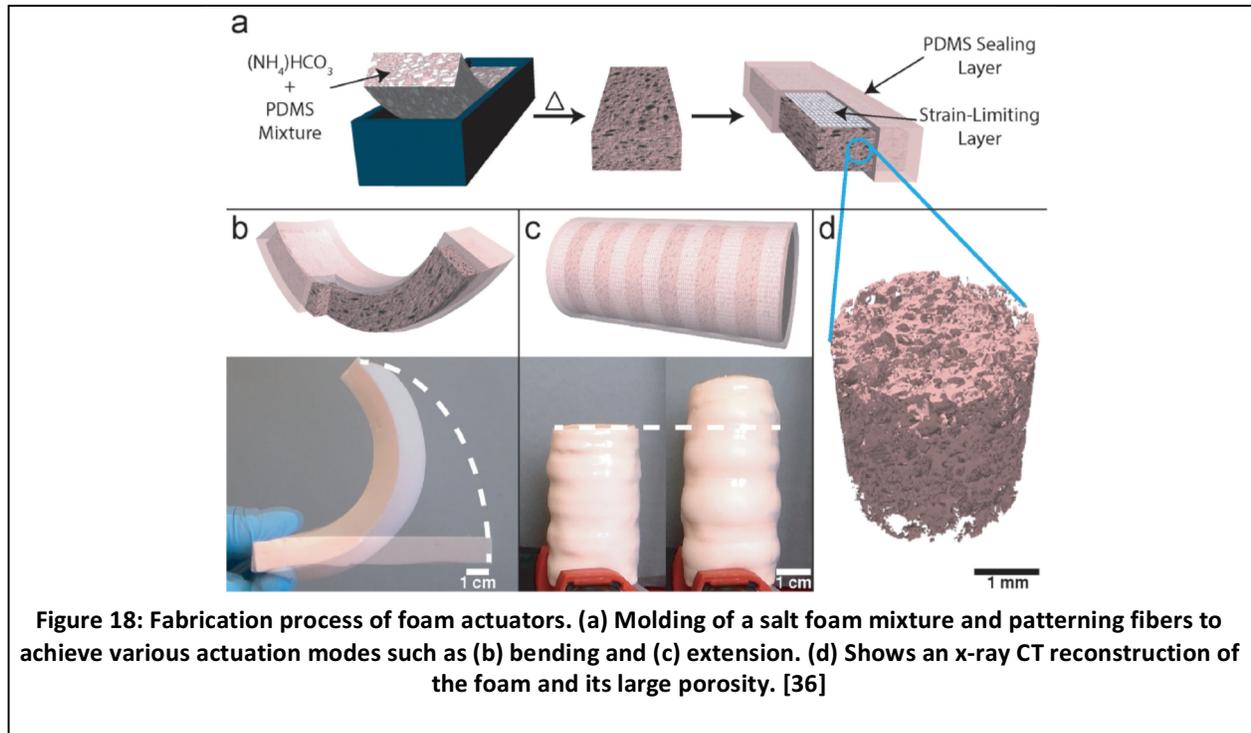
Figure 18: Fabrication process of foam actuators. (a) Molding of a salt foam mixture and patterning fibers to achieve various actuation modes such as (b) bending and (c) extension. (d) Shows an x-ray CT reconstruction of the foam and its large porosity. [36]

Machine body. Previously, Co-I Shepherd has fabricated silicone based robots that can jump,[1, 2] walk,[3, 4] and navigate obstacles.[3, 5] The largest of these soft robots is 0.7m in length and operates untethered, powered pneumatically by on-board air compressors using lithium-polymer battery packs.[5] The actuators that comprise these machines are reliable and have been tested over one million cycles Figure 17 with very little change in performance (i.e., actuation speed and displacement; see above figure for Pressure vs Volume curve of a soft actuator at one actuation cycle and 1M cycles).[6] The complexity of the lamprey rover's proposed shape, however, has made it difficult to simply assemble these actuators into the envisioned shape. Even though the robotic lamprey is inspired by a relatively simple animal, there is significant three-dimensional complexity to our proposed design. Instead of using the useful but limited pneumatic actuators in Figure 17, we have developed an entirely new soft actuator technology capable of forming highly complex body and actuator architectures.

During the NIAC Phase I performance period, we have demonstrated the ability to use foam rubber as, simultaneously, the body and actuators of soft robots. This ability has been demonstrated in two recent publications by Shepherd,[7, 8] (Figure 18) one funded by the Phase I NIAC award ([35];Figure 19).[7] In these demonstrations, we use additive manufacturing to form soft machines from elastomeric foam (Figure 18,Figure 19).

Figure 19: Mold free, rapid fabrication of foam machines. (left column) Sculpting of a loch ness monster and (right column) curvature vs. pressurization of a foam tentacle. [35]
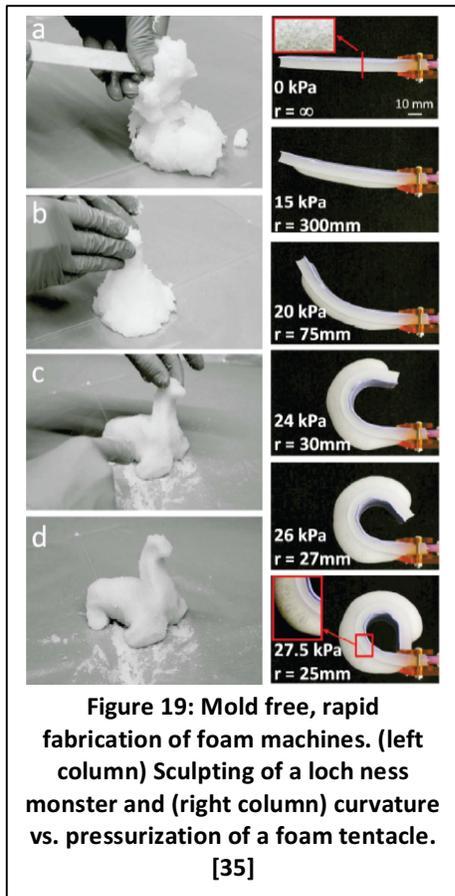
We have further developed the foam actuator process by pursuing direct injection molding of thermoplastic polyurethanes. The benefits of using this process are two-fold: (i) injection molding requires only seconds to form a machine and (ii) can produce small (mm) and large (m) scale bodies. The shape and motions of the proposed rover will be defined by the foam and will comprise, by volume, ~80% of the uninflated, uncompressed robot's body. Since 80% of the foam is empty volume, there is the potential that our ~0.5m x 0.5m x 1.0m, 0.25 m^3 rover could be stored in a 0.04 m^3 volume, taking into account all of the incompressible structures (e.g., valves and fuel cell). Further, since 80% of the 0.25 m^3 is pore space, then the mass of the body will only account for a few hundred grams.

In Phase I, we have started to mold foam actuators in the form of the robotic lamprey's body. Figure 20a,b shows a bidirectional foam actuator we expect will form the lamprey's tail, and its ability to actuate at large amplitudes. Figure 20c shows that these foams can be greatly compressed for transport and Figure 20d,e shows the combustion powered hydrojetting chamber can also be used for buoyancy control. While this buoyancy control is a huge advantage of our rover, it also poses a control challenge: actuation will also change the buoyancy of the rover. During Phase II, we will form the robotic eel's entire body and integrate all of the subsystems. While the buoyancy control issue is complex, the ability to selectively store gas and actuate different components of the robot should provide a solution.

While we are still pursuing the lamprey, we have also begun exploring a glider design similar to that presented in Ref. [9] that would ride ocean currents and use buoyancy control to slowly drift over large distances for long periods of time. We believe our inflatable machine structure is perfectly suited to achieve long duration underwater exploration via gliding.

11.4   Buoyancy

Cornell University
College of Engineering

Diving deep beneath the ice to the ocean floor can be easily achieved with low amounts of power by changing the buoyancy of the system by manipulating the average density of the rover. This same mechanism can be similarly used to rise from the ocean depths. Remarkable velocities can be achieved dependent upon the aerodynamic of the rover enabling a dive of hundreds of kilometers to happen within hours. A reasonable rise time of 1 m s^{-1} can travel 1000m in under 7 minutes. A dive of 100 km can occur in 28 hours.

A model of the buoyant force of a silicone balloon was created using the Mooney Rivilin model for biaxially strained hyperelastic materials. The model can be used to derive buoyant force and the associated energy cost for inflating that balloon. The equation for the number of moles of gas in the balloon as a function of r is given in (15 where n is the number of moles of gas, C_{01} is a material constant of Ecoflex 30 Silicone set as 11.75 kPa, V_b is the initial material volume, R is the universal gas constant, T is the temperature of the gas, and r is the current radius.

$$n = \frac{C_{01} * V_b}{R * T} \left(\frac{r}{r_{init}}^4 - 2 * \frac{r}{r_{init}}^{-2} \right) \qquad \textbf{(15)}$$

Using this model of a hyperelastic material, a model for a balloon volume and balloon pressure has been developed. Basic manipulation using material properties of the silicone, electrolysis ideal energy cost, experimentally determined fuel cell efficiencies, external pressure at STP, and the displaced water volume results in a model of Buoyant Force vs Energy. Assuming a spherical elastomer with thickness of 5mm and initial radius of 5cm that weighs 0.1854Kg, the buoyant force per electrolysis energy input is as shown in Figure 21.
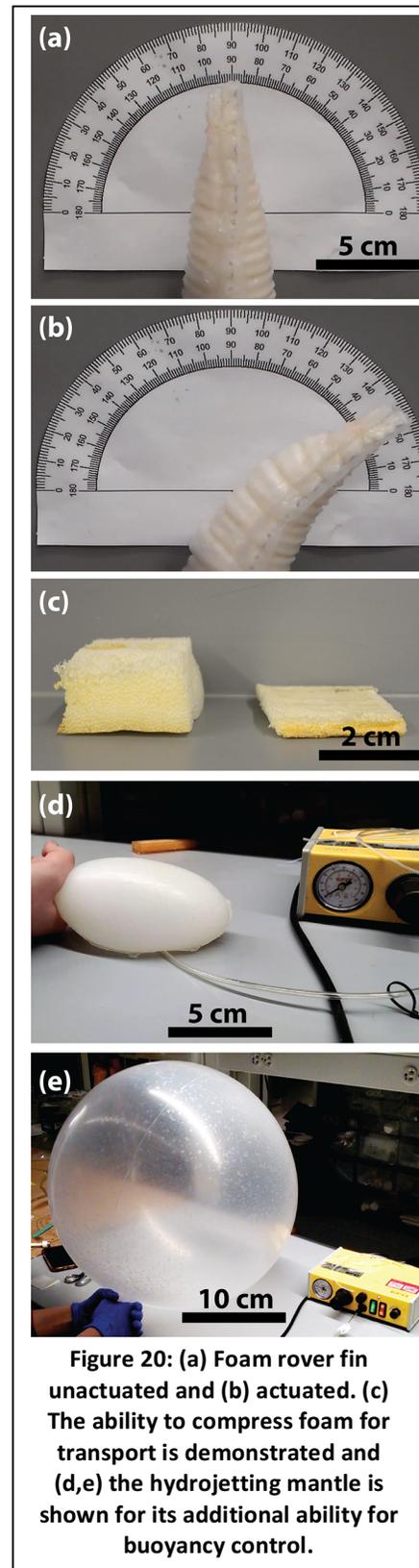
Figure 20: (a) Foam rover fin unactuated and (b) actuated. (c) The ability to compress foam for transport is demonstrated and (d,e) the hydrojetting mantle is shown for its additional ability for buoyancy control.

Figure 21: Buoyant Force vs Energy with Fracture circle indicated (above) Maximum Mantle Inflation Prior to Failure in Test to Failure (below)
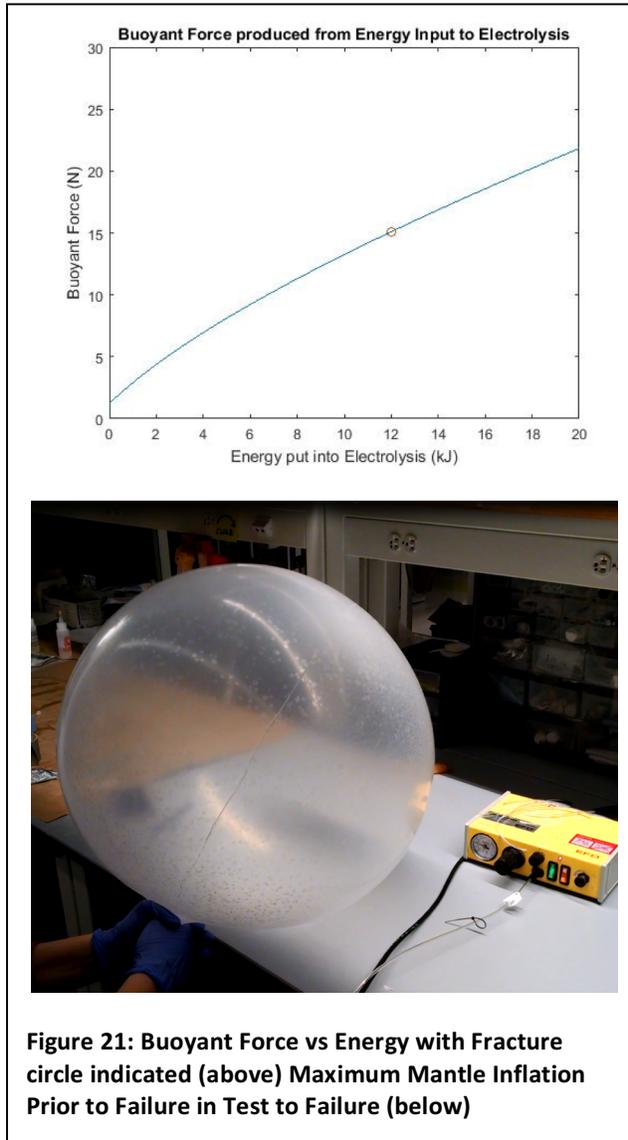
This model assumes atmospheric pressure and energy input will increase as external pressure increases. The red circle indicates the fracture point of the material at approximately 15N. This force in the 1.315 m/s^2 Europa Gravity can lift 11Kg. Note that the balloon modeled weighs approximately 184grams and the balloon in the image is approximately 200grams. Note that there exist better elastomers with significantly higher strain rates than the one used that should be investigated as well as the effects of Europa water pressure on energy. The only force acting against this form of locomotion is the required energy to inflate a balloon under high pressures which could exist on Europa.

The water pressure predicted for Europa has a large spread based on the technique used to estimate ocean pressure. The water pressure has been predicted to be 5 atm assuming 3 km thick ice crust, 150 bar assuming 150 km thick ice, and 30 bar assuming 50 km of ice. The pressure is mainly dependent upon ice crust depth which models predict to be anywhere between 2 km and 150 km using different methods. The primary impact of such large uncertainty in the pressure variation on the rover will be the amount of energy and time necessary to generate buoyancy and actuate soft mechanisms that operate based on pressure difference.

It should be noted that the gas used in filling this balloon is not lost. The soft rover will be capable of repurposing this gas after filling its balloons for use in soft actuators, hydrojetting, or powering its sensors.

11.5 Water Jet Propulsion

A major result from our Phase I study is that electrolysis from a fuel cell consuming 1 W can produce enough fuel and oxidant for significant combustion powered hydrojetting. Further the rapid deflagration of hydrogen was capable of propelling a synthetic mantle. Figure 22 shows the concept for combustion powered hydrojetting in the robotic lamprey and a prototype of the hydrojetting mantle. The hydrojetting chamber is modeled after the mantle of an octopus, which squeezes water into a jet that propels it backwards. By fixing a deformable, synthetic mantle on the interior of our combustion chamber, the ignition of combustible fuel causes the mantle to deform and squeeze out water, causing propulsion. Figure 22,right column shows high speed camera footage of the hydrojetting system moving at a speed of 3 m s^{-1}, fully submerged under water. This is remarkable for many reasons, one is that the mantle was actually fixed in place to measure the force exerted. The thrust force generated was enough to dislodge it from its fixture.

Figure 22: Electrodynamic tether and H2 and O2 gas generator subsystem.

11.5.1 Combustion

The idea behind combustion of oxyhydrogen is the opportunity to achieve rapid propulsion in short bursts, possibly for sample collection using a beak at the tip of the rover for collecting mass spectrometer samples. The primary purpose of this testing is to develop a propulsion mechanism that uses the energy released from the combustion of hydrogen and oxygen gasses. We are trying to determine the maximum efficiency of such a waterjetting system, the dependence of efficiency on geometry, the maximum velocity that can be achieved and what design achieves that velocity.

Presently, the combustion chambers are clear rigid plastic nalgene bottles. These bottles are clear so the glow plug ignition can be observed in the video, during testing, and so the internal dynamics of the water jetting bladder can be observed. The long term objective is to convert the entire system into a flexible mantle that can be compressed.

11.5.1.1 Combustion Science

Combustion is a complex combination of chemical and thermal models that can be used to model the pressure and volumetric properties of the gasses. Theoretical models explaining the pressure volume relationship of a gas with a non-rigid boundary condition can be derived in future studies. For now, our testing revolves around the combustion of oxyhydrogen. This ratio promises to have the maximum

power output given our input. It may be beneficial to change this equivalence ratio to reap the benefits from longer burn times and flame speeds of the hydrogen and oxygen combustion. We additionally believe that the permeation of this gas in foams will decrease the flame speed and the phases of the combustion reaction long enough to increase the amount of power harvested from the rapid hydrogen oxygen combustion. These effects have been left to Phase ll studies.

11.5.1.2 Ignition

There are two primary methods of ignition that are being pursued, glow plug and spark ignition. The concept behind both is to create a local increase in temperature above the flash point of the gas resulting in combustion.

The glow plug operates at approximately 12V and 3 amps. This is a very power hungry further testing needs to be done to determine the minimum energy input necessary to produce combustion. This is also a very reliable method of combustion. What can occasionally occur between ignitions is the condensation of the water vapor byproduct on the glow plug and internals of the chamber. This result in the glow plug first evaporating the water vapor before heating the H_2 and O_2 gasses and producing combustion. If enough water has accumulated from multiple combustions without purging the chamber, this water could prevent the combustion from taking place entirely by forcing the submerged glow plug to vaporize all the water.

The alternative combustion ignition is the sparking caused by arcing due to high voltage potential differences using capacitors to store charge over time. This method could be far better in the future as the heating is caused by the local high temperature plasma in the arc between anode and cathode. This could be as simple as running several leads to different parts of the chamber and igniting them at different times. Sparks can even occur when fully submerged and partially submerged.

11.5.2 Experimentation

11.5.2.1 Experiment Setup

The experimental setup has been designed to measure the energy input to the chamber and force output of an elastomer water jet propulsion mechanism. The energy input is measured in 3 ways. The first method is through the voltage and current input to the rover. The second is through the hydrogen gas input with volumetric flow meters. The third is gas input from the oxygen volumetric flow meters. Either volumetric flow can be used because they should be being produced in stoichiometric quantities, ensuring that each test is completely oxyhydrogen to maximize energy output.

Cornell University
College of Engineering
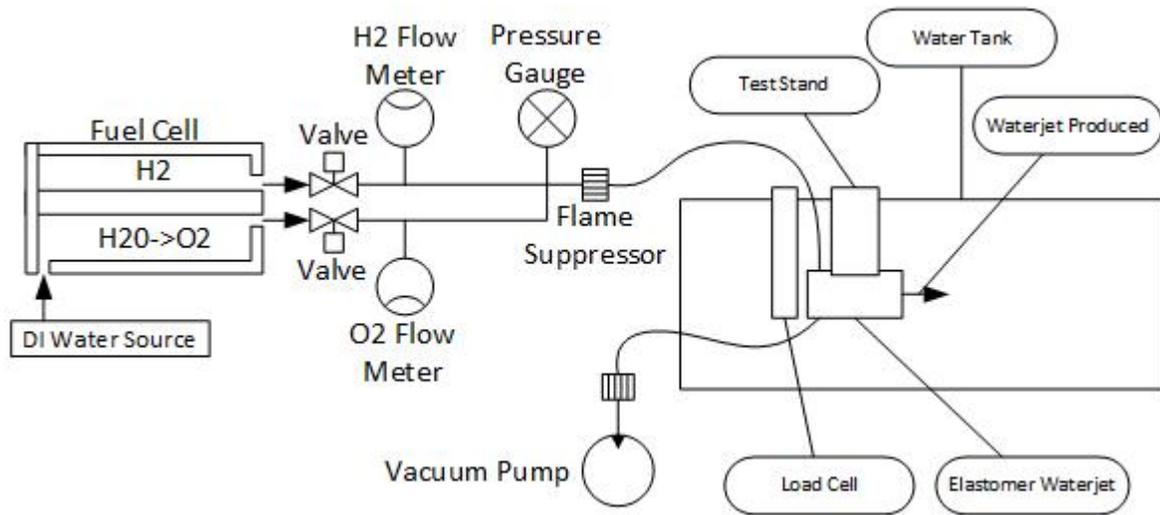
Figure 23: Water Jet Propulsion Force and Mobility Test Stand

Fuel cells were used to generate the hydrogen and oxygen gas for these tests. The fuel cells used were Horizon Technology PEM Fuel Cells meant for educational demonstrations and cost less than $50. The electrical energy input to the fuel cells was indirectly measured through voltage and current through known loads. Additionally, two pressure based flow meters were used to measure the standard cubic centimeters of hydrogen and oxygen produced. A pressure gauge was placed in series and is used to determine when a pressure equilibrium is reached between the inside of the elastomer waterjet and the atmosphere. A load cell is used to determine the propulsive force generated by the the waterjet. Finally, a high speed camera captures the dynamics of the waterjetting process and is capable of indicating everything from the volumetric expansion rate of the gas, strain rate of the elastomer, and velocity of the combustion chamber.

The process for measuring the force output by the elastomer hydrojet and energy input is as follows:

1. A vacuum pump is used to remove a majority of the gas from the chamber typically down to -0.7psi. This removes the gasses contained in the hoses and elastomer waterjet which contain a combination of oxygen, hydrogen, water vapor, water, nitrogen, and the other trace elements that constitute air. This is not sufficient to pull a complete vacuum, but removes some of the remnant gasses.
2. The fuel cells are powered until they have produced the desired volume of gas
3. The voltage applied to the fuel cells is measured
4. The voltage drop across a known resistance in series with the fuel cells is measured
5. The power to the fuel cells are turned off
6. The Hydrogen gas and Oxygen gas supply valves are closed
7. The gas supply data is saved
8. The load cell data collection is turned on
9. The Glow Plug ignition switch current limiter is removed

10. The high speed camera begins recording
11. The gas is ignited
12. The high speed camera recording is saved
13. The load cell data is saved

Occasionally, the gas does not initially ignite and a second recording must occur.

After the first combustion of the day, the following anomalies tend to occur that change the dynamics of the test. The gas in the chamber has lots of condensation and water vapor from the previous combustion that adds to the residual gasses in the test. This may contribute to subsequent tests occurring at lower expansion times than the first test. The glow plug is also often coated in water. In order for the H2 and O2 gas to combust, the glow plug must run long enough for the water droplets condensed on the surface of the glowplug to evaporate and the local concentration of H2 and O2 to reach the minimum ignition concentration.

The load cell data is limited in rise time and peak time by the amplifier used.

11.5.2.2 Experimental Results

11.5.2.2.1 Unconstrained Hydrojet Powered Mantle Motion
In order to determine a rough order of magnitude of the velocity a hydrojetting mechanism could achieve, the test setup in Figure 23 was modified by removing the load cell. Using the high speed camera, frame by frame motion of the mantle was recorded and can be observed in **Error! Reference ource not found.**(a). From this high speed imagery, velocimetry can be performed to determine the velocity of the mantle. The maximum velocity of the mantle and bladder is 200 in s^{-1} or 0.5 m s^{-1} . It should be noted that this bladder burst during the test as the high velocity mantle pulled the thin walled silicone bladder into the sharp edge of the test stand holding it in place. Careful observation of the T=20 ms frame shows the bladder's contact with the test stand. Based on the propagation of gas in T=40ms, it is clear that this was the cause of the failure.

The flow meters indicate a hydrogen gas input of 189.69 scc(standard cubic centimeters) at STP. Using the ideal gas law, the total number of moles of hydrogen gas is estimated to be 0.0078 moles. Using the same method on the oxygen flow meter resulted in the expected 0.0039 moles, exactly half that of the hydrogen gas. By back calculating the number of moles of gas and using 80% efficiency of our fuel cells, the energy input to the system is 3.54 kJ. Running this combustion in Europa's ocean will take slightly less than 1 hour with a 1 watt electrodynamic tether.

It is worth noting that the bladder inside the mantle as indicated in Figure 24(c) is approximately 4 inches long initially and cylindrical in shape with 0.3175 cm wall thickness. As Figure 24(c) shows, the bladder is not in a cylindrical shape at the beginning of the test due to acting on the water in the bladder. This is an important observation as the high speed images at T=20ms and T=30ms. This indicates that even the small pressure difference between the bottom and top of the mantle, a 5cm height difference, indicates an uneven expansion of the bladder. This expansion of the bladder could be caused by three different sources (i) initial
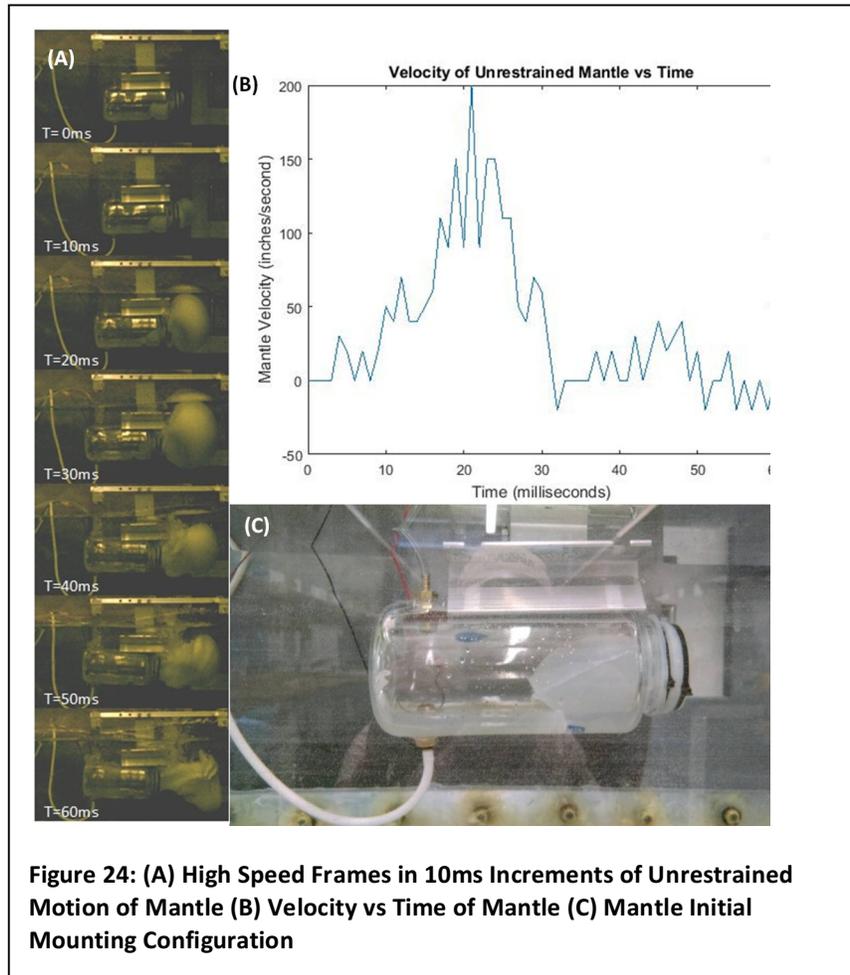
Figure 24: (A) High Speed Frames in 10ms Increments of Unrestrained Motion of Mantle (B) Velocity vs Time of Mantle (C) Mantle Initial Mounting Configuration

alignment of the bladder due to gravity acting on the higher density water that vectors expansion upwards (ii) buoyant forces acting on the bladder during the gas expansion phase of combustion resulting in upward motion and (iii) the local high pressures in the water tank experimental setup. Phase ll will need to investigate these possibilities and others in order to achieve directed motion of hydrojetting.

11.5.2.2.2 Restrained Mantle with Completely Internal Bladder Test

In this experiment, the bladder indicated in Figure 25 was mounted internally to the mantel as in Figure 24(B) but this bladder filled more of the system internals. Using the test setup from Figure 23, the force output in Figure 25 was generated. The maximum impulse generated by this combustion is 0.4973 Ns. This is enough impulse to propel the current combustion chamber design at approximately 2.56 m s^{-1} assuming no drag.

Figure 25: Large Bladder Force Output over Time under Hydrojetting (Left) Large Bladder to be placed in the mantle
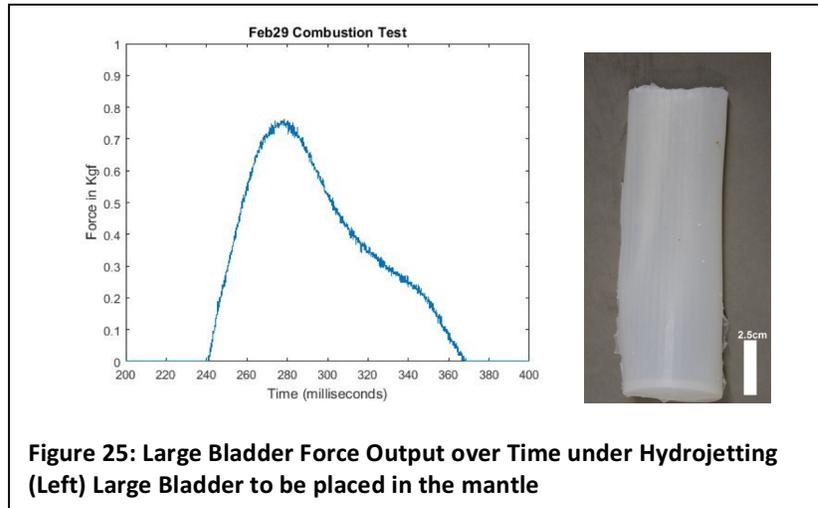
In this experiment, the total gas flow rate of H2 was 165.5 scc. The total energy input via volumetric flow rate is 3.09 kJ, meaning there are 0.0068 moles of H2 in the system and 0.0034 moles of O2 in the mantle for this combustion.

11.5.2.2.3   Restrained Mantle with Partially Internal Bladder Test

In this experiment, the bladder is folded on itself in the entrance of the bottle. This folding may allow for more rapid volume increases of the silicone material than when the bladder is located entirely inside the mantle. The impulse delivered by this mantle in this combustion experiment is 0.79 Ns. This is enough to propel the current 0.194 g chamber design at approximately 4 m s^{-1}. The total volumetric flow of hydrogen into the system is 151.689 scc of H2 gas which implies that 0.0063 moles of H2 gas at stp entered the system and 0.0031 moles of O2 gas entered the system. The total energy estimated by volumetric flow is 2.836kJ. The total energy input estimated using the voltage drop across a known load is 1.952kJ. The maximum thrust produced is 10.58N. It is important to note that this experiment was divided into two data sets as the gas generation was halted partway through the process.

Figure 26: Mantle Hydrojetting time series of a 15.24cm long bladder with radius 5cm(left) and Mantle Force vs Time Plot (right)
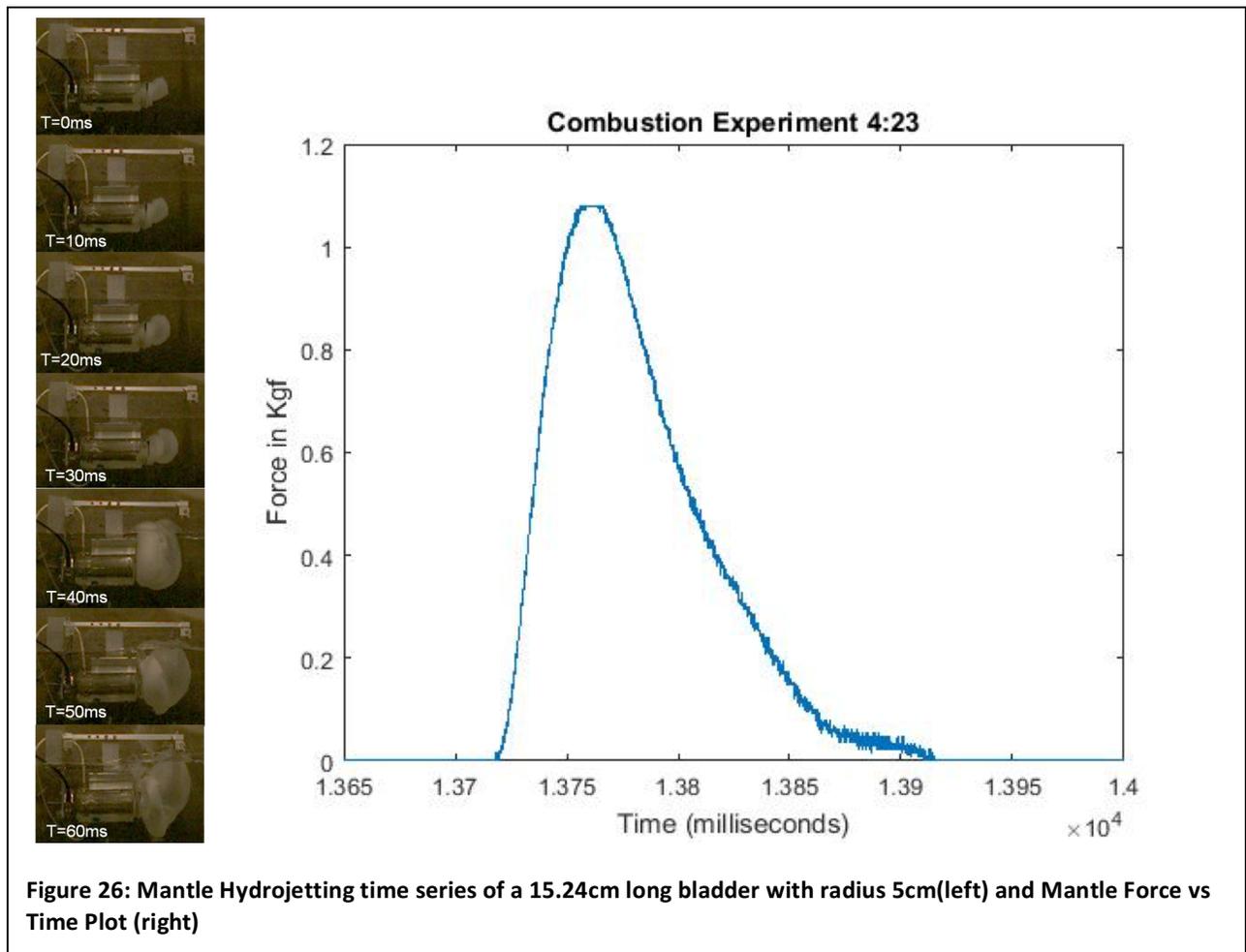
The experiment with the large bladder entirely internal to the mantle produces an impulse of 0.4973 Ns with 3.09 kJ of energy input. The experiment with the large bladder folded in the nalgene bottle restriction produces a larger impulse of 0.79 Ns at a lower energy input of 2.863 kJ. These results indicate that the propulsion produced by rapid shape change is dependent upon the rate of shape change which is dependent upon initial geometry of the system. A focus of Phase ll may be to

investigate geometries that naturally revert to their initial shapes but are capable of large shape changes.

12   Conclusion

The Phase I results show that a soft robotic, underwater rover has many advantages over a traditional view of autonomous underwater vehicles. Many of these advantages stem from its ability to collapse or expand the body, which carries two key benefits: (i) cost savings in transport and (ii) buoyancy control. Furthermore, this rover's material offers properties that enable it to survive most oceanic conditions, withstand a likely radiation environment, and retard ice formation. The use of these soft robots under water is very attractive because buoyancy enables very large robots without the need for skeletal structures that limit their shape-changing ability.

The theoretical calculations and experimental investigation on electrodynamic tethers discussed in this report show that their use in saltwater environments is feasible. However, magnetohydrodynamic effects require attention, which will be a priority in Phase II. A possible approach involves magnetic shielding of a portion of the EDT array to generate significant current from imposed alternating magnetic fields. The Phase I experiments show that this approach may enable enough power to be generated for a soft robotic rover of the scale contemplated here. This power is in the range of 1mW to 1W and determines the time required to collect and transmit science data. The prime limitation of soft robots for underwater exploration is their nascent state of development, an issue that this study has begun to address and that we hope to continue in Phase II.

Cornell University
College of Engineering

13   Bibliography

[1 R. S. Mason Peck, "Soft-Robotic Rover with Electrodynamic Power Scavenging," Cornell University,
]   Ithaca, 2015.

[2 National Aeronautics and Space Administration, "Outgassing Data for Selecting Spacecraft
]   Materials," 13 January 2016. [Online]. Available: https://outgassing.nasa.gov/. [Accessed 30 January
    2016].

[3 M. H. Carr, M. J. S. Belton and e. al, "Evidence for a subsurface ocean on Europa," *Nature,* vol. 391,
]   pp. 363-365, 1997.

[4 P. Plait, "Huge lakes of water may exist under Europa's ice," Discover, 17 November 2011. [Online].
]   Available: http://blogs.discovermagazine.com/badastronomy/2011/11/17/huge-lakes-of-water-
    may-exist-under-europas-ice/#.Vt5PD_krKM8. [Accessed 9 January 2016].

[5 O. L. Kuskov and V. A. Kronrod, "Internal Structure of Europa and Callisto," *Icarus,* 2004.
]

[6 H. J. Melosh and e. al, "The Temperature of Europa's Subsurface Water Ocean," *Icarus,* 2003.
]

[7 J. J. Petrovic, "Mechanical Propeties of Ice and Snow," *Journal of Materials Science,* vol. 38, pp. 1-6,
]   2003.

[8 K. M. Soderlund, B. E. Schmidt and e. al, "Ocean-driven heating of Europa's icy shell at low
]   latitudes," *Nature Geoscience,* 2013.

[9 National Aeronautics and Space Administration, "NASA Facts: Mars Pathfinder," 1997.
]

[1 National Aeronautics and Space Administration, "Europa Study 2012 Report: Europa Lander
0] Mission," 2012.

[1 J. Hagerty and J. C. Rogers, Spaceship Handbook, ARA Press, 2001.
1]

[1 C. Gebhardt, "SLS upper stage proposals reveal increasing payload-to-destination options," NASA,
2] 12 November 2013. [Online]. Available: http://www.nasaspaceflight.com/2013/11/sls-us-proposals-
    increasing-payload-destination-options/. [Accessed 12 January 2016].

[13] W. Zimmerman, R. Bonitz and J. Feldman, "Cryobot: An Ice Penetrating Robotic Vehicle for Mars and Europa," in *IEEE Aerospace Conference Proceedings*, 2001.

[14] K. Cooper, "Tunneling Cryobot Robot May Explore Icy Moons," *Astrobiology Magazine,* 12 June 2015.

[15] Stone Aerospace, "News: Stone Aerospace wins Phase 2 funding for Project VALKYRIE," 2011 October 18. [Online]. Available: http://www.stoneaerospace.com/. [Accessed 2016 January 13].

[16] C.-J. Chang, "Electrodynamic Behavior of PMG-Delta," Naval Postgraduate School, Monterrey, 1994.

[17] P. Schenk, F. Nimmo and L. Prockter, "Europa's Icy Shell: A Bridge Between Its Surface and Ocean," *Eos Transactions American Geophysical Union,* p. 311, 17 August 2004.

[18] "Vision and Voyages for Planetary Science in the Decade 2013-2022," National Academies, Washington D.C., 2011.

[19] C. Zimmer, "Subsurface Oceans on Europa and Calisto: Constraints from Galileo Magnetometer Observations," *Icarus,* vol. 147, pp. 329-347, 2000.

[20] D. Schulze-Makuch and I. N. Louis, Life in the Universe: Expectations and Constraints, Berlin: Springer, 2004.

[21] M. L. Cosmo and E. C. Lorenzini, Tethers in Space Handbook, Washington D.C.: National Aeronautics and Space Administration, 1997.

[22] W. B. Russel, D. A. Saville and W. R. Schowalter, Colloidal dispersions, Cambridge University Press, 1992.

[23] Magnetic Shield Corp., "Science, Research, and Education from Magnetic Shield Corporation Science and Research," Magnetic Shield Corp., [Online]. Available: http://www.magnetic-shield.com/science-research-and-education.html. [Accessed 2016 March 9].

[24] Lenntech, "Water Conductivity," Lenntech, [Online]. Available: http://www.lenntech.com/applications/ultrapure/conductivity/water-conductivity.htm. [Accessed 9 March 2016].

[25] R. G. C. Zheng Ouyang, "Miniature Mass Spectrometers," *Annual Review of Analytical Chemistry,* vol. 2, pp. 187-214, 2009.

[26] S. Fanali, Liquid Chromatography Applications, Elsevier Science, 2013.

[27] "ChemWiki: 11D Voltammetric Methods," University of California Davis, [Online]. Available: http://chemwiki.ucdavis.edu/Analytical_Chemistry/Analytical_Chemistry_2.0/11_Electrochemical_Methods/11D\%3A_Voltammetric_Methods.

[28] F. Arianpour, "Water and ice-repellent properties of nanocomposite coatings based on silicone rubber," University of Quebec, 2010.

[29] Shin-Etsu Silicone, "Characterstic Properties of Silicone Rubber Compounds," Shin-Etsu Silicone, 2005. [Online]. Available: http://www.shinetsusilicone-global.com/catalog/pdf/rubber_e.pdf. [Accessed 18 January 2016].

[30] G. De Angelis, M. S. Clowdsley, J. E. Nealey, R. K. Tripathi and J. W. Wilson, "Radiation analsis for manned mission to the Jupiter system," *Advances in Space Research,* vol. 34, pp. 1395-1403, 2004.

[31] E. Howell, "Could ionized gas to a better job of sterilizing spacecraft?," Astrobiology Magazine, 24 February 2015. [Online]. Available: http://www.astrobio.net/news-exclusive/ionized-gas-better-job-sterilizing-spacecraft/. [Accessed 18 January 2016].

[32] "The Outer Space Treaty of 1967," NASA History Program Office, 26 October 2006. [Online]. Available: http://history.nasa.gov/1967treaty.html. [Accessed 9 March 2016].

[33] M. Calisti, M. Giorelli, G. Levy, B. Mazzolai, B. Hochner, C. Laschi and P. Dario, "An octopus-bioinspired solution to movement and manipulatio for soft robotics," *IOP Publishing,* 2011.

[34] University of South Florida, "Scientists discover secret to highly efficient swimming in some animals such as jellyfish," 2015. [Online]. Available: http://phys.org/news/2015-11-scientists-secret-highly-efficient-animals.html. [Accessed 22 Janurary 2016].

[35] A. Argiolas and e. al, "Sculpting Soft Machines," *Soft Robotics.*

[36] B. C. Mac Murray and e. al, "Poroelastic Foams for Simple FAbrication of Complex Soft Robots," *Advanced Materials,* vol. 41, no. 27, pp. 6334-6337, 2016.

[37] B. Mosadegh and e. al, "Pneumatic Networks for Soft Robotics that Actuate Rapidly," *Advanced Functional Materials,* vol. 24, no. 15, pp. 2163-2170, 2014.

[38] M. Manga and C. Y. Wang, "Pressurized oceans and the eruption of liquid water on Europa and Enceladus," *Geophysical Research Letters,* vol. 34, 2007.

[39] Z. Ouyang and G. R. Cooks, "Miniature Mass Spectrometers," *Annual Review of Analytical Chemistry,* vol. 2, pp. 187-214, 2009.